Magneto-optics of two-dimensional electron systems in the ultraquantum limit: incompressible quantum liquids and the Wigner crystal

I. V. Kukushkin and V. B. Timofeev

Institute of Solid State Physics, Russian Academy of Sciences, Chernogolovka, Moscow Region
(Submitted 4 March 1993; resubmitted after revision 7 April 1993)
Usp. Fiz. Nauk **163**, 1–28 (July 1993)

Radiative recombination of 2D electrons with photoexcited holes in a single GaAlAs–GaAs heterojunction is used to illustrate the possibilities of the magneto-optic approach to the investigation of the ground state of strongly-correlated electrons in the ultraquantum limit. The method is used to determine the Coulomb gaps of quantum liquids and their hierarchy in the fractional quantum Hall effect. Wigner crystallization of 2D electrons is investigated and an analysis of time-resolved recombination spectra is used to reconstruct the phase boundary of the Wigner crystal.

1. INTRODUCTION

Several events associated with the discovery of some striking physical phenomena have taken place during the last decade in the physics of low-dimensional semiconducting systems. The integral quantum Hall effect (IQHE)[1] was discovered in 1980. Two years later, and before its significance was fully understood, the *fractional* quantum resistance[2] was discovered. Today, almost ten years later, we are confronted by one further surprise, namely, the discovery of the crystal phase of two-dimensional electrons—the so-called Wigner crystal. The aim of this review is to familiarize the reader with magneto-optic studies of these phenomena. Magneto-optics has been found to be a particularly effective tool in the experimental investigation of Coulomb correlation effects in an interacting 2D electron gas.

We note, at this point, that the quantum Hall effect, subsequently refered to as the integral QHE, is a magnetotransport phenomenon in two-dimensional electron (hole) layers in metal–insulator–semiconductor (MIS) structures, and also in heterostructures with modulated dopant concentration.[3,5] The effect is seen phenomenologically by applying a strong enough magnetic field **B** perpendicular to the plane of free motion of the 2D electrons, and is accompanied by the appearance of plateaus on the Hall resistance (ratio of transverse voltage to the longitudinal count). The zeros of longitudinal resistance correspond to the Hall plateaus at $T=0$. The phenomenon is fully correlated with the appearance of single-particle gaps in the spectrum of 2D electrons in a magnetic field, namely, the cyclotron, spin, and valley-orbital gaps that confine the electrons to Landau orbits with energies $E_n=(n+1/2)\hbar\omega_c$, where ω_c is the electron cyclotron frequency. The Hall conductivity σ_{xy} in the case of the integral QHE, i.e., on the plateaus, is very precisely given by

$$\sigma_{xy}=\nu e^2/h, \tag{1.1}$$

where e and h are universal atomic constants and ν is the filling factor. The filling factor is defined by

$$\nu=N_s/N_0, \tag{1.2}$$

where N_s is the density of 2D electrons and $N_0=1/2\pi l_0^2=eB/h$ is the maximum permissible electron population or the capacitance of the quantum state [$l_0=(\hbar/eB)^{1/2}$ is the magnetic length]. The most striking feature of the integral QHE is that the plateaus of σ_{xy} and the zeros of σ_{xx} occur for the integral values $\nu=...4, 3, 2, 1$. The conditions $\nu\leqslant 1$ refer to the quantum limit.

The integral QHE is a single-electron phenomenon and is due to the specific structure of the 2D electron spectrum in a transverse magnetic field in the presence of a random potential, i.e., practically all the states in the energy gaps are highly localized (in the spirit of the Anderson localization) and the nondissipative Hall current transports a few (1 at $T=0$) delocalized extended states.[3,5] The high precision of quantization of Hall conductivity in (1.1) is due to the fact that the conductivity of all 2D systems can be represented by a topological invariant that is independent of the random potential of the defects that are always present in real 2D systems.[3]

The discovery of the fractional quantum Hall effect two years after the discovery of the integral effect was totally unexpected. It was considered that, as the quality of the samples improved (structures with better separation boundaries, more uniform electric potentials confining carriers in 2D planes, and so on), and also as the quantum region $\nu<1$ byond the limit is reached, one should be able to see the crystallization of electrons, i.e., the two-dimensional Wigner crystal.[6,7] This type of crystallization had been seen earlier in the classical limit for the 2D electrons on the surface of liquid helium.[7] However, for perfect structures with 2D electron gas and high quantum mobility, the magnetotransport curves were found to display a fine structure that was not directly related to Wigner crystallization. In particular, new plateaus and zeros were found in the magneto-transport parameters, i.e., in conduc-

 1063-7869/93/070549-23$10.00

tivity and resistivity, for fractional filling factors $\nu=p/q$ where p is an integer and q an odd integer. This phenomenon was subsequently called the fractional quantum Hall effect (FQHE). It was found that FQHE could be observed at much lower temperatures than the integral quantum Hall effect. This clearly demonstrated that the energy spectrum of 2D electrons contained totally new gaps that could not be understood within the framework of this simple single-electron description. Soon after, the QHE was explained[8] as being a consequence of an interaction between electrons that produces highly correlated many-electron states (the so-called Laughlin states), often referred to as incompressible quantum liquids (QL). Such states constitute a liquid because they do not display long-range order among the electrons, and the incompressibility is understood in the sense that a change in density or filling factor would require an energy comparable with the corresponding gap that separates the ground state of the QL from the continuum of quasiparticle excitations. According to Laughlin's theory,[8] such unusual states of the electron quantum liquid occur exclusively for rational fractional filling factors $\nu=1/q$ with even denominators. In accordance with the electron-hole symmetry, the hole states of the QL exist for $1-(1/q)$. In the many-electron theory,[8,9] quasiparticle excitations carry the fractional charge $e^*=e/q$ in FQHE. In contrast to the single-electron gaps (cyclotron, spin and valley-orbital) of the integral QHE, the fractional QHE involves Coulomb gaps that are due to the interaction between the particles. The scale of a Coulomb gap, Δ_2, is determined by the fractional charge and decreases with increasing q in accordance with the expression

$$\Delta_q \approx 0{,}1e^{*2}/\varepsilon l_0 = 0{,}1e^2/\varepsilon q^2 l_0 \sim q^{-5/2}H^{1/2}, \qquad (1.3)$$

where ε is the permittivity of the medium. The quantities Δ_q are very small, so that the QL is a very delicate substance in the QHE regime. It is therefore not surprising that such states have been found only in high-grade structures containing the 2D electron gas, in which the random potential does not destroy these states (the necessary electron mobilities are of the order of 10^6 cm^{3}V^{-1}s^{-1} or more) and, in addition, the necessary temperatures are very low (of the order of 1 K or less). Despite the stringency of these conditions for the observation of FQHE, whole families of such states have been found in magnetotransport experiments[10,11] and the hierarchy of these families has been established up to $\nu=1/7$, in accordance with the theoretical predictions.[12]

The odd denominator rule is a consequence of the Pauli principle and is due to the antisymmetric many-electron wave function that describes the ground state of the QL which, in the Laughlin theory, consists of electrons with the same spin projection. Subsequent experiments demonstrated (well after this was shown theoretically in Ref. 13) that, in principle, the ground state of the QL can be a singlet (in contrast to the spin-oriented Laughlin state) and consists of electrons with opposite spin directions.[14,15] Quasiparticle excitations above the gaps can subsequently occur with spin flip. In these special cases, in which there are additional spin degrees of freedom, and which we shall not pause to consider in detail, rational fractions can be observed under the conditions of the FQHE with even denominators. The odd denominator rule is therefore hardly universal in FQHE.

In the colorful and strikingly successful history of the fractional quantum Hall effect, the question that has become increasingly topical is: where is the Wigner crystallization of 2D electrons and when does it occur? This problem has become particularly accute after reliable numerical calculations have defined more accurately the region in which the proposed crystallization can occur ($\nu_c \leqslant 1/5$, Ref. 16). It is important to remember that it is simply unrealistic to expect that direct experiments based on the elastic scattering of neutrons or X-rays will provide a direct demonstration of long-range order in an interacting system of 2D electrons. Nevertheless, different and methodologically independent recent experiments (studies of radiofrequency absorption,[17] magneto-transport,[18,19] sound absorption,[20,92] magneto-optics,[21] and also cyclotron resonance[93]) have provided substantial evidence (though not direct evidence) for the existence of this crystallization. As we enter the ultraquantum region ($\nu \ll 1$) and the region of low temperatures, increasingly strong localization on fluctuations in the random potential ensures that electrons lose their ability to traverse macroscopic distances. This means that the magnetotransport method encounters fundamental difficulties in this region because the system containing the 2D electron gas begins to resemble more and more a dielectric, and becomes more like an electron glass.

We now turn to the magneto-optic method for which strong localization effects do not constitute such a strong limitation. It is well-known that radiative recombination of 2D electrons and nonequilibrium holes injected in some way into the system can be used as a basis for measuring the electron energy spectrum. It is, of course, assumed in this approach that the energy spectrum of the holes is known in detail. We shall be interested in systems with a single 2D electron channel. They are encountered in MIS-structures and heterostructures. The electric potential that confines the 2D electrons to the neighborhood of the interface and repels nonequilibrium holes from the separation boundary into the interior (buffer) region. However, because the wave function of the 2D electrons extends in the direction perpendicular to the interface, radiative electron-hole recombinations still have a finite probability. This is the basis of the luminescence method for the direct measurement of the single-particle density of states of 2D electrons in Si–MIS structures[22,23] and the single GaAlAs–GaAs heterojunction.[24] The method has been successively used under the conditions of the integral QHE to measure the size of energy gaps in the single-particle electron spectrum in a transverse magnetic field, the density of quantum states during variations in their filling, nonlinear screening of fluctuations in the random potential, and so on (see the review literature[24–26]).

However, the efficacy of the luminescence method in FQHE is not obvious at first sight. Actually, the nonequilibrium holes, i.e., effectively charged particles, should first

produce a strong perturbation of the delicate system that is the quantum liquid under the QHE conditions. Next, it is not clear *a priori* whether it is possible in an optical experiment with 2D systems of this kind to achieve the low temperatures indicated by the scale of the Coulomb gas (1K or less) and whether the system of 2D electrons will be in quasiequilibrium under such conditions? Finally, the above luminescence method leaves unanswered questions such as the disposition of the nonequilibrium holes, with which electrons recombine, relative to the 2D electron channel. These complications can be overcome by using specially fabricated structures containing the 2D electron gas. When such objects are chosen for magneto-optic studies, preference must be given to semiconducting systems with well-defined asymmetry in the electron–hole interaction. A successful object of this kind can be a single heterojunction in which the two-dimensional electron channel is spatially separated by a region occupied by photoexcited holes. It is desirable to have these holes 'attached' to acceptor centers that lie at a sufficiently long and fixed distance from the interface. Such structures can be implemented, for example, in the single GaAlAs–GaAs heterojunction with an acceptor δ-layer 'built in' by molecular-beam epitaxy and modulated doping at the required distance from the interface. Since the acceptor is neutral and distant from the interface, there is minimum masking of Coulomb correlations by the excitonic effect under the conditions of FQHE and Wigner crystallization. We note that in systems that are symmetric in the electron–hole interaction, e.g., in quantum-wells, the influence of exitonic effects is very considerable. If the electrons and holes are not spatially separated, the excitonic effect completely compensates Coulomb correlations in the electron subsystem and, as a consequence, such correlations do not appear in the corresponding luminescence spectra.

Our review is arranged as follows. In Section 2, we consider the foundations of the magneto-optic method that relies on the radiative recombination of 2D electrons with photoexcited holes localized on acceptor centers (BE atoms) in the δ-layer of the single GaAlAs-GaAs heterojunction. Studies of the single-particle energy spectrum of 2D electrons in a strong transverse magnetic field are presented in Section 3. The magneto-optics of 2D electrons in FQHE is discussed in Section 4 where it is shown that the magneto-optic method can be used to explore the ground state of interacting electrons by varying the filling of the quantum states, and the efficacy of optical measurements of the quasiparticle Coulomb gaps is demonstrated. Finally, Section 5 describes optical experiments involving the Wigner crystallization of 2D electrons in a strong transverse magnetic field. It is shown that pulsed photoexcitation and analysis of time-resolved recombination spectra can be used to distinguish between the crystalline and disordered (glassy) electron phases and, in the final analysis, construct a phase diagram for the Wigner crystal.

2. RADIATIVE RECOMBINATION OF 2D ELECTRONS IN A SINGLE HETEROJUNCTION

It is well-known that the spectroscopic method employing the radiative recombination of 2D electrons and photoexcited holes is successful in studies of the electron energy spectrum. The method is particularly widely used in the case of quantum wells (QW) containing a 2D electron gas [see, for example, (27) and (28) and also the review given in Ref. 29]. When we are interested in Coulomb correlations between 2D electrons, it is better to use the single heterojunction than the quantum well. There are several reasons for this. First, the radiative time constant for the QW is of the order of a nanosecond or less in the case of semiconductors in which optical transitions are allowed in the zero order in the wave vector **k**. Sufficiently low electron temperatures (of the order of 1K or less) cannot be produced in such systems with such short radiative recombination time constants. Second, photoexcited holes and electrons are not spatially separated in the symmetric quantum well, so that the excitonic effect in such systems compensates Coulomb correlations in the 2D electron gas. Finally, the properties of the QW, e.g., the electron mobility, are inferior as compared with the single heterojunction structure. This is due to the presence of the reverse heterojunction in the QW whose structure is inferior to that of the direct heterojunction.

These defects and limitations are practically absent from specially fabricated GaAlAs–GaAs n-type heterostructures with an acceptor δ-layer at a considerable distance Z_0 from the region occupied by the 2D electrons. The energy scheme for this type of heterostructure is illustrated in the insert in Fig. 1. They are grown by molecular epitaxy.[30] Diffusion effects and the subsequent spreading of the acceptor monolayer can be avoided by using low enough grid temperature and low dopant concentration in the δ-layer ($\leqslant 10^{10}$ cm^{-2}). In contrast to the quantum well, high grade structures with very high mobility of 2D electrons (of the order or greater than 10^6 cm^{2}V^{-1}s^{-1}) can be produced in single heterojunctions with δ-doped layers.

Radiative recombination of 2D electrons and holes in acceptor centers localized in the δ-layer is usually investigated in such structures by photoexcitation that generates nonequilibrium electron–hole (e,h) pairs near the heteroboundary.[31] The surface concentration of acceptors in a monolayer is lower by almost two orders of magnitude than the concentrations of 2D electrons, so that the radiative recombination process does not affect the electron density. Figure 1 shows the luminescence spectra of GaAlAs–GaAs heterostructures for different distances of the acceptor δ-layer (Be atoms) from the heteroboundary.[32] For comparison, the figure also shows the spectrum of a single heterojunction without special δ-doping. In this structure, the B-band is due to the residual density of acceptor centers (C atoms) in the buffer GaAs region. The bands A_1, B_1, and B_0 in these spectra represent the recombination of 2D electrons with free holes (A lines) and holes in acceptor centers (B lines) (the subscripts indicate the band number in the dimensional quantization of the 2D electrons).[31] The B_1 and B_0 line inten-

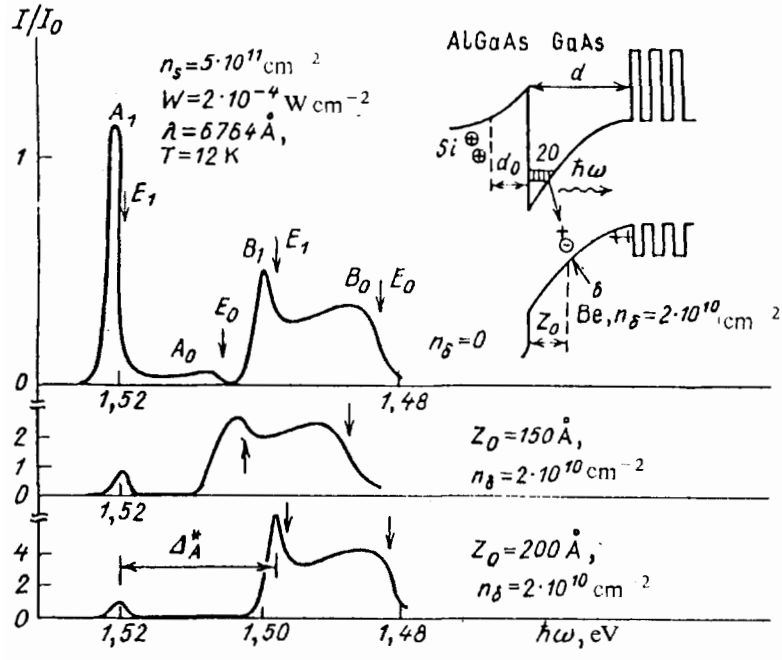

FIG. 1. The luminescence spectra of GaAlAs–GaAs heterojunctions with different distances Z_0 of the δ-layer of acceptors from the heteroboundary. The insert shows heterojunction configuration. The top spectrum was obtained without special δ-doping.

sities are normalized to the A_1 intensity measured under identical conditions. It is clear that when the acceptor δ-layer is closer to the heteroboundary, B-line intensity is higher. At the same time, the B lines are broadened and their position on the energy scale is very dependent on Z_0. The changes in the positions of the B lines in the spectrum is due to changes in the binding energy of the acceptors in the δ-layer as the distance Z_0 is varied (Stark effect[32]).

Let us now consider the shape of the luninescence spectrum due to the radiative recombination of 2D electrons with holes in acceptors in the δ-layer (B_0 lines). The shape of the spectrum can be accurately represented by the convolution of single-particle densities of state of electrons and holes $D_{e,h}(E)$, their distribution functions $f_{e,h}(E)$, and the optical transition matrix element

$$I(\hbar\omega) \sim \int_0^\infty D_e(E)\, D_h(\hbar\omega - E) f_e(E) f_h(\hbar\omega - E)\, dE. \tag{2.1}$$

Momentum is conserved in direct radiative recombinations of 2D electrons and acceptors because of the recoil of the impurity center, and the transition matrix element is practically independent of energy. The density of states of holes and their distribution in the δ-layer can be represented by a δ-function with sufficient precision. The shape of the B-line luminescence spectrum then directly reflects the single-particle density of states of the 2D electrons for a given equilibrium filling function $f_e(E)$:

$$I(E) \sim D_e(E) f_e(E). \tag{2.2}$$

In zero magnetic field, this spectrum is rectangular in shape, reflecting the constant density of states of the 2D electrons ($D_e = m/\pi\hbar^2$), and its total width at half height at $T=0$ is equal to the Fermi energy of the 2D electrons. Such rectangular spectra had been observed earlier for Si–MIS-structures.[22,23] The 2D electron wave function has the following form in the direction of dimensional quantization:

$$\psi_{0,1}^{2D}(Z) \sim \exp[-Z(2mE_{0,1})^{1/2}/\hbar], \tag{2.3}$$

where E_0 and E_1 are the effective potential-barrier heights for the ground and first excited dimensional quantization subbands. The B_0 and B_1 line intensities can be used by varying Z_0 to analyse the tails of the wave functions (2.3) and to determine, among other things, the barrier heights $E_{0,1}$ (Ref. 32). The probability of radiative recombination of a 2D electron and a hole in an acceptor center in the δ-layer is determined by the corresponding overlap of their wave functions, i.e., $w_R \sim |\langle \psi_e^{2D}(Z) | \psi_h^A \rangle|^2$. It is clear that the radiative recombination probability should decrease exponentially with increasing Z_0, so that the radiative time constants should correspondingly decrease. Figure 2 shows the luminescence decay time constant measured for the 2D electrons in the ground band of dimensional quantization under pulsed laser excitation in different structures with $Z_0 = 250$, 300, and 350 Å. The radiative time constant increases, as expected, by almost an order of magnitude. The function $\tau(Z_0)$, which is determined by the change in the overlap of the electron and hole wave functions, can be used to deduce the coordinate dependence (in the Z-direction) of the 2D electron wave function.

The time constant for the radiative recombination of 2D electrons in the ground subband and holes bound to acceptors in the δ-layer is thus of the order of 10^{-6} s. The corresponding time constant for electrons in the first excited subband is smaller by approximately an order of magnitude because of the long tail of the wave function in this state, other things being equal. This constitutes a radical difference between these heterostructures and the recombination of 2D electrons with free holes in quantum wells in which $\delta \approx 10^{-9}$ s (Ref. 35). This means that, in a single

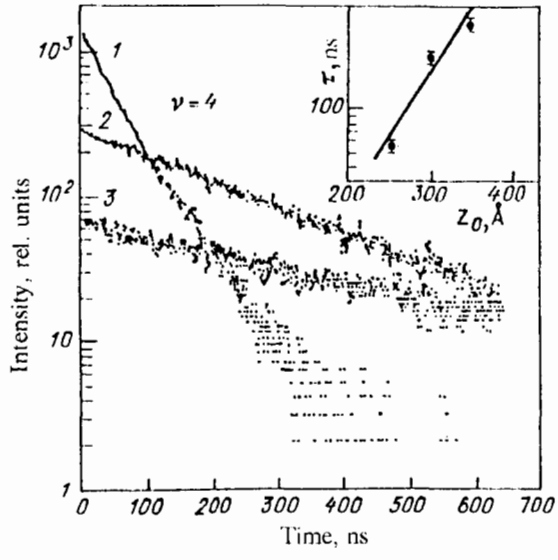

FIG. 2. Decay of the luminescence intensity due to 2D electrons in the ground subbands o dimensional quantization under pulsed laser excitation. 1, 2, and 3 correspond to the following distances between the acceptor δ-layer and the interface, respectively: Z_0=250, 300, and 350 Å. The insert shows the function $\tau(Z_0)$.

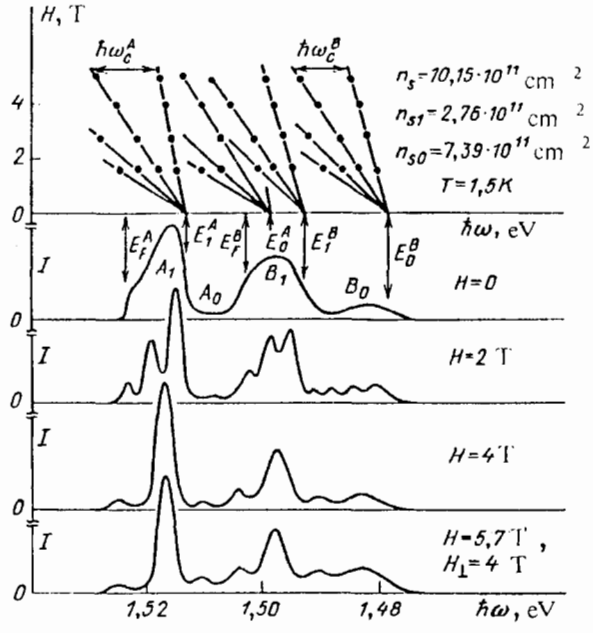

FIG. 3. Luminescence spectra due to 2D electrons in a single GaAlAs–GaAs heterojunction in a perpendicular magnetic field and also in a field H=5.7 T and 45° to the 2D plane.

GaAlAs–GaAs heterojunction with an acceptor δ-layer, the superheating of the electron system in an optical experiment is smaller than in the quantum well.

We now turn to the question of a possible variation in the concentration of 2D electrons in a single GaAlAs–GaAs heterojunction by photoexcitation of nonequilibrium e, h pairs near the heteroboundary. It has been shown experimentally[36] that when continuous illumination is used to create carriers in the $Ga_xAl_{1-x}As$ layer (photon energy greater than the direct band gap of $Ga_xAl_{1-x}As$ for given composition x), a significant change can be achieved in the stationary concentration of 2D electrons when the power density is high enough. This experimental fact is explained qualitatively by saying that the nonequilibrium holes produced by illumination travel towards the heteroboundary in which they recombine with the 2D electrons. At the same time, some of the injected electrons are trapped by ionized residual donor centers in the region of the spacer (undoped GaAlAs layer near the interface). Both processes produce a reduction in the stationary concentration of 2D electrons and, in the final analysis, the quantum well containing the electrons becomes wider and shallower. The significant point is that the injection of nonequilibrium e, h pairs is accompanied by a considerable reduction in the concentration of 2D electrons (by a factor of between 1 and 10) and an increase in their mobility. The latter phenomenon is due to the fact that the resulting number of charged centers near the heteroboundary decreases under illumination. These qualitative considerations have recently been described analytically,[37] and the results are in agreement with experiment.

3. MAGNETO-OPTICS OF 2D ELECTRONS IN IQHE

We now consider the radiative recombination of 2D electrons in a single heterojunction in a transverse magnetic field in the case of IQHE. When the magnetic field is applied, the density of states of the 2D electrons (if we neglect spin) is a set of δ-function peaks separated by $\hbar\omega_c$. Each Landau level is degenerate and its capacity is determined by the magnetic length. In real 2D systems with disorder, the interaction between electrons and the random potential lifts the degeneracy, and the Landau levels acquire a finite width. For example, in the case of short-range scattering centers, the single-particle density of states in the wings of the Landau levels is described by[4]

$$D(E)\sim\exp(-E/2\Gamma)^2, \tag{3.1}$$

where $\Gamma\approx\hbar\omega_c/(\mu H)^2$ and μ is the electron mobility. The distribution of the density of states is determined by the nature of the inhomogeneities and by the screening of their potential, which in turn depends on the filling factor. This information is particularly significant for the microscopic description of magnetotransport properties of 2D electrons in a wide range of variation of the filling factor. The advantages of the magneto-optic method, to which we shall return later, include the fact that it can be used to find the total-energy distribution for a single-particle density of states, directly under the Fermi level, to determine the single-particle gaps in the energy spectrum and their behavior as the filling factor is varied, and to examine the random potential itself, i.e., its amplitude and linear scale.

3.1. Luminescence spectra of 2D electrons in the single GaAlAs–GaAs heterojunction in a transverse magnetic field

An example of this spectrum is shown in Fig. 3 in which we can clearly see the Landau splitting of the A_i and B_i lines. The splittings are proportional to the normal component of the magnetic field. The dependence of the spec-

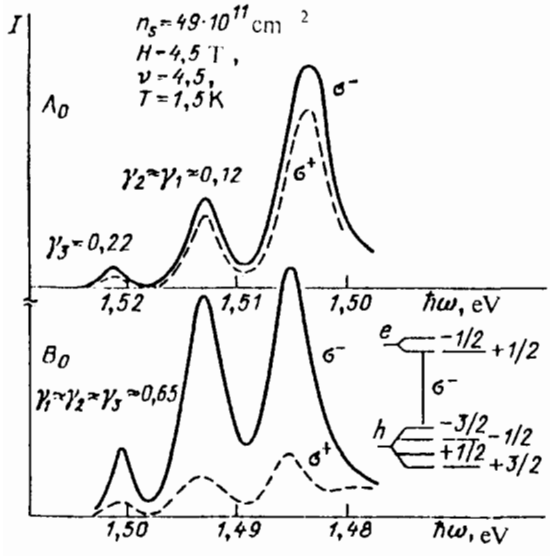

FIG. 4. Polarized luminescence due to 2D electrons a magnetic field, measured in the Faraday geometry.

tral positions of the lines split by the magnetic field on the field H is shown by the fan of Landau levels at the top of the figure. These diagrams can be readily used to locate the bottom of the dimensional quantization band and the position of the Fermi level on the energy scale (indicated by the arrows in Fig. 3).

The Landau splittings are different for A_i and B_i lines. The effective cyclotron mass found from A_i line splitting is $m_c^* = 0.06m_0$, whereas the B_i line splitting gives $0.067m_0$ which is very close to the cyclotron mass of 2D electrons in the single GaAlAs–GaAs heterojunction. These differences are due to the fact that the resultant splittings in the case of A_i lines include contributions due to free holes, i.e., heavy holes ($m_h^H = 0.57m_0$). The two-dimensional character of the electrons that recombine with the holes is indicated by the splitting of the A_i and B_i lines in the inclined field. Figure 3 shows that the splitting of the A and B lines is sensitive only to the normal component of the magnetic field.

3.2. Optical polarization in the spectra

When the temperature is low enough, the luminescence spectra observed in a magnetic field are polarized as a result of spin splitting in the 2D electron and hole subsystems. Figure 4 illustrates the splittings and the optical transitions in the case of recombination with a neutral acceptor center. It also shows the A_0 and B_0 luminescence spectra recorded in Faraday geometry for σ^0 and σ^+ polarizations. It is clear that the B_0 line has a high circular polarization. In accordance with selection rules, the spectra become completely σ^- polarized if $\mu_0 g_{e,h} H \gg kT$ and if the nearest electron and hole sublevels are populated (as a result of recombination between an electron with spin projection $S_z = +1/2$ and a hole with angular momentum z-component $J_z = -3/2$).

The circular polarization measured in different magnetic fields at different temperatures is well-described by the expression

$$\gamma = \frac{1-\exp(-\Delta E_s/kT)}{1+\exp(-\Delta E_s/kT)}, \tag{3.2}$$

where $\Delta E_s = 2\mu_0 g_h H$ is the Zeeman splitting between hole levels with $J_z = -3/2$ and $J_z = +1/2$, and g_h is the g-factor of a hole in the acceptor. This dependence is approximately represented by taking the g-factor of a hole in the acceptor to be $g_h = 1.1$.

The polarization of the A_0 line for $H < 10$ T is much smaller than the polarization of the B_0 line (see Fig. 4). This result is due to the mixing of the spin states of light and heavy holes. We note, finally, that the circular polarization is not the same for different Landau levels, but increases as they approach the Fermi level. This is due to the spin polarization of the 2D electrons in the upper Landau level, which is a maximum for odd filling factors $\nu = ...5, 3, 1$.

3.3. Oscillations and enhancement of the electron g-factor

As in the case of Si–MIS structures, radiative recombination in a single GaAlAs–GaAs heterojunction at sufficiently low temperatures involves 2D electrons with only one spin projection, i.e., $S_z = +1/2$ (filling factors $2m < \nu < 2m+1$; $m = 0, 1, 2, ...$). In measurements of spin splitting, the temperature can be increased to achieve sufficient population of the Zeeman sublevels of the acceptor center ($J_z = \pm 3/2, \pm 1/2$). The spectra then acquire a component with the other electron spin projection, namely, $S_z = -1/2$. This was in fact the approach adopted in the case of the Si–MIS structures.[38-39] There is, however, another way of measuring the spin splitting. It is based on an analysis of the variation in the position of a luminescence line in a magnetic field at low temperatures T. We note that the enhancement of spin splitting ($\mu_0 \Delta g_{eff}^e H$) occurs only for levels close to the Fermi level, since it is only then that there can be appreciable differences between the populations of the corresponding spin states ($\Delta N \equiv N_\uparrow - N_\downarrow \neq 0$). The change in the spin splitting of the 2D electrons due to the exchange interaction is described by

$$\Delta E_{spin} \approx \Sigma_{exch} \frac{N_\uparrow - N_\downarrow}{N_\uparrow + N_\downarrow} \approx \frac{e^2}{\varepsilon l_0} \frac{\Delta N}{N_\uparrow + N_\downarrow} \equiv \mu_0 \Delta g_{eff} \cdot H, \tag{3.3}$$

where Σ_{exch} is the exchange integral. Hence, it follows that the enhanced g-factor ($\Delta g_{eff} \sim \Delta N H^{-1/2}$) should oscillate as the filling of the magnetic sublevels is varied (g_{eff} is a maximum for strictly odd ν). Figure 5a shows the position of the luminescence lines (A components) as a function of the magnetic field (or ν). For $\nu = 3, 5, 7, ...$ and, in particular, near the Fermi level, ΔE ceases to be the linear function caused by cyclotron splitting. This is due to spin splitting associated with volume effects. Specifically, $\Delta E = -1/2\mu_0 \Delta g_{eff} H$ and is unrelated to the renormalization of the gap. Below the Fermi level, the Landau level shift is a linear function of H, and the Landau level sepa-

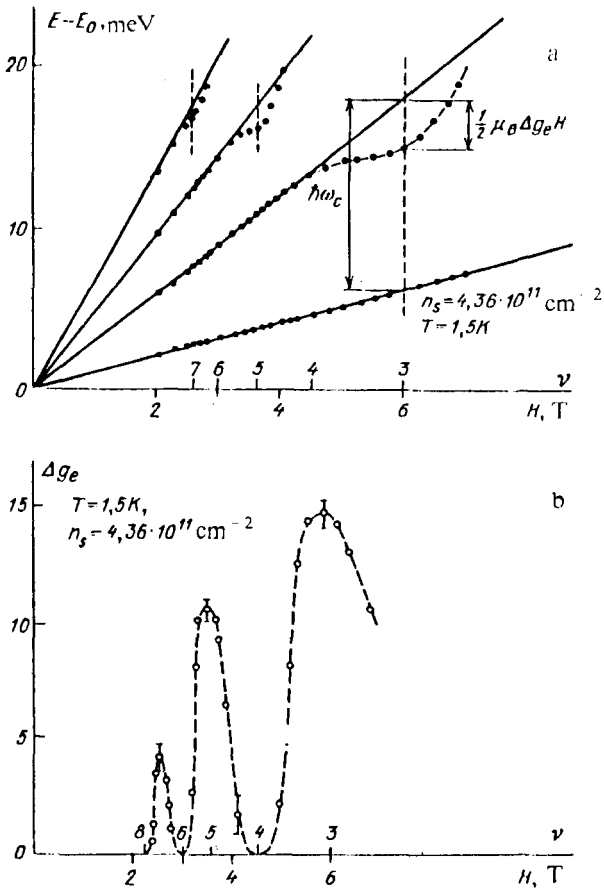

FIG. 5. Center of gravity of a luminescence line (A_0 component) as a function of the magnetic field H or filling factor ν for $n_s=1.36\times10^{11}$ cm^{-2}, $T=1.5$ K. E_0 is the bottom of the dimensional quantization band. b—Oscillations in the g-factor of 2D electrons, enhanced by the exchange effect. $n_s=4.36\times10^{11}$ cm^{-2}, $T=1.5$ K.

ration is strictly equal to $\hbar\omega_c$. The oscillating dependence of Δg_{eff} on ν measured by this method is shown in Fig. 5b, from which it is clear that Δg_{eff} is a maximum for $\nu=3$, 5, 7,... . For example, in the above experimental situation, the magnitude of Δg_{eff} for $\nu=3$ is greater by a factor of almost 30 as compared with the bulk value of g for an electron in GaAs ($g_0=-0.4$).

3.4. Spin relaxation of photoexcited electrons and holes

In the magneto-optic method discussed above, we have considered the relaxation of the electron–hole system in respect of all the degrees of freedom, including spin, during photoexcitation. The point is that we need to know the relation between the interband and spin relaxation time constants for the 2D electrons and holes in the acceptor center, on the one hand, and the radiative recombination time constants, on the other. Without this information it is difficult to judge the equilibrium or otherwise of the 2D electron and hole systems, and the electron temperatures that can actually be attained in an optical experiment.

This information was recently obtained by studying the kinetics of circularly polarized magnetoluminescence of single GaAlAs–GaAs heterojunctions under pulsed laser excitation with monsecond resolution.[40,41] Radiative recombination of 2D electrons from Landau levels in the ground subband (B_0 line) and the first excited subband (B_1 line) was investigated. In the ground subband, the Landau levels are completely filled, i.e., the populations of the two spin components are equal, so that the circular polarization of the B_0 line is determined exclusively by the state of the hole spin subsystem. The B_i line polarization includes contributions of both hole and electron spin orientations, which in the final analysis can be separated. Figure 6 shows the polarization due to the holes (curve γ_h) and the resultant contribution of electrons and holes to this polarization (curve γ_e) as functions of time. It is clear that, even for zero delays, the electron system exhibits appreciable polarization. The observed reduction in the electron contribution to the polariation is due to the establishment of electron spin equilibrium. Thereafter, when the curves γ_e and γ_h in Fig. 6 become parallel, it may be considered that the electron contribution has ceased to vary.

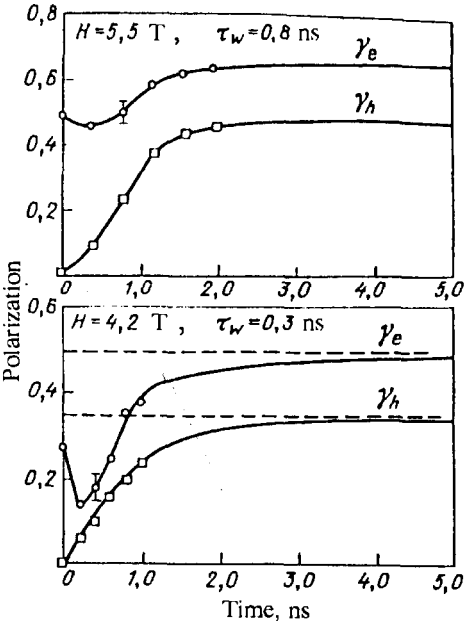

FIG. 6. Circular polarization of luminescence as a function of time, determined by holes (γ_h) and electrons (γ_e).

The following sequence of relaxation time constants was finally established experimentally for the above system: the shortest were the time constants obtained for the interband electron relaxation with conservation of spin projection (less than 0.3 ns). The next was the time constant for establishing electron spin equilibrium (of the order of 0.5 ns); finally, the time constant for the spin relaxation of holes in the acceptor was about 2 ns. All these time constants are shorter by at least two orders of magnitude than the time constant for radiative recombination from the ground 2D electron subband. Equilibrium is established in the system for these values of the relaxation and radiative recombination constants. The single heterojunction with an acceptor δ-layer has undoubted advantages from this point of view as compared with symmetric quantum wells for which the electron (hole) relaxation and

recombination time constants are not very different.

3.5. Magneto-optic oscillations in the intensity of recombinational emission

So far, we have been concerned with the behavior of the resultant spectrum due to the radiative recombination of 2D electrons with photoexcited holes, which reflects the properties of the single-particle density of states above the Fermi level in a magnetic field. On the other hand, it is well-known that quantization of the motion of electrons ensures that the thermodynamic and kinetic variables oscillate as functions of the magnetic field (this is seen, for example, in the Shubnikov–de Haas effect). By direct analogy with this, one would expect that the luminescence intensity corresponding to the recombination of 2D electrons near the Fermi level should also oscillate as a function of the magnetic field. There have been several recent publications on this optical analog of the Shubnikov–de Haas oscillations, observed in the magnetic-field dependence of the intensity of recombinational emission by 2D electrons.[42–46] The intensity of magnetoluminescence from the first excited subband with nonequilibrium population has been investigated for 2D electrons recombining with free holes (quantum well[43], single heterojunction[44]) and with holes in acceptor centers (single heterojunction with an acceptor δ-layer[45,46]). In the case of recombination with free holes, the magnetic-field dependence of the luminescence intensity is found to exhibit sharp peaks that correspond exactly to integer filling factors of 2D electrons in the ground subbands. This effect is explained by the screening of the Coulomb potential of photoexcited holes by 2D electrons.

The magneto-optic oscillations may also be due to another effect associated with the complicated kinetics of relaxation processes under photoexcitation. In particular, when the system is subjected to continuous photoexcitation it can be in a nonequilibrium (but stationary) state and the observed line intensity can be determined not only by the equilibrium thermodynamic distribution of particles, but also by the relaxation kinetics of the nonequilibrium component of the electron gas. The magnetic-field dependence of the line intensities, due to transiently occupied states, will therefore contain valuable information not only about the energy spectrum, but also about the character of the relaxation processes involving 2D electrons in the quantizing magnetic field. This situation was examined in Ref. 45 which reported an experimental study of magneto-oscillations in the luminescence emitted by 2D electrons from transiently filled first excited subband of dimensional quantization in the case of recombination with holes bound to acceptors (neutral centers). Magneto-oscillations in the luminescence from the first excited subband are shown in Fig. 7a. The lower part of this figure shows the band of Landau levels obtained by analyzing the resultant luminescence spectra in a magnetic field. It is immediately clear that the oscillation peaks do not lie strictly in accordance with the integer filling factors established by independent experiments with the same illumination, using the minima of the Shubnikov oscillations in magnetoresistance. It is also clear that there is a one-to-one correspondence between the position of the signal edges on the luminescence peaks (indicated by downward arrows) and the crossing of the corresponding Landau levels, namely, the ground subband and the zeroth Landau level of the first excited subband. The mechanism for this is most likely to be elastic relaxation of carriers from a subband with nonequilibrium filling to the ground subband. The perturbation that mixes the wave functions of different subbands can then be provided by the residual-impurity atoms near the 2D channel. This interpretation is confirmed by experiments on the optical detection of cyclotron resonance.[47]

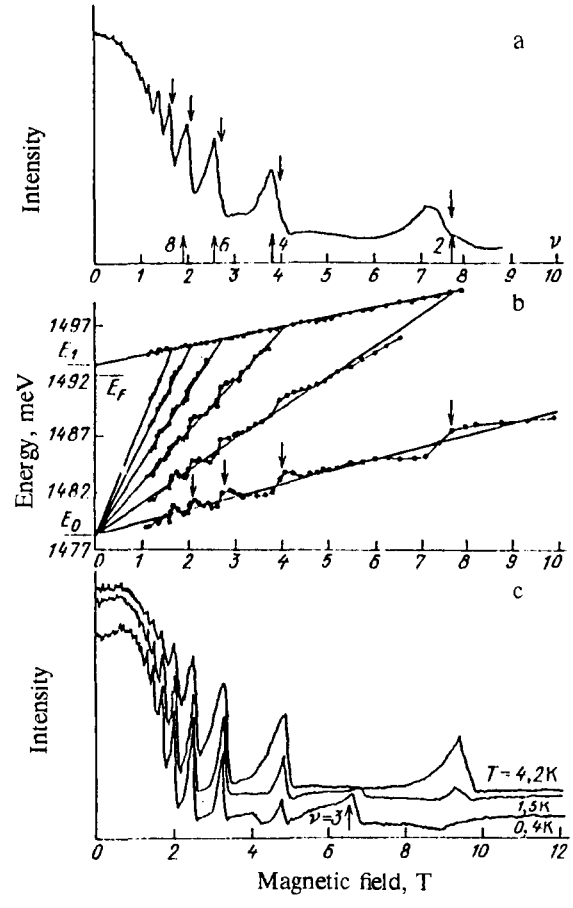

FIG. 7. a—Radiative recombination intensity due to 2D electrons from the first excited subband as a function of magnetic field for $\varepsilon_F < \varepsilon_{10}$. b—Position of Landau luminescence peaks as a function of magnetic field. Downward arrows show the crossings of the zeroth Landau level of the excited band and the levels of the ground subband. Upward arrows—even filling factors. c—Buildup of spin states at lower temperatures.

These magneto-oscillations in luminescence intensity are very sensitive to temperature. For relatively high T, the oscillation peaks correspond to even ν, whereas at lower temperatures, peaks with odd filling number begin to dominate the magneto-oscillation phenomenon (Fig. 7c). This effect is explained by the enhancement of spin splitting at lower temperatures. For example, $g_e\mu H > kT$ for $T \approx 0.4$ K, so that a significant difference between the populations of spin sublevels in the ground subband is found to arise, and this in turn leads to an effective increase in spin splitting because of the enhanced exchange interaction. All this means that, for odd ν, the vacancies, i.e., unfilled positions

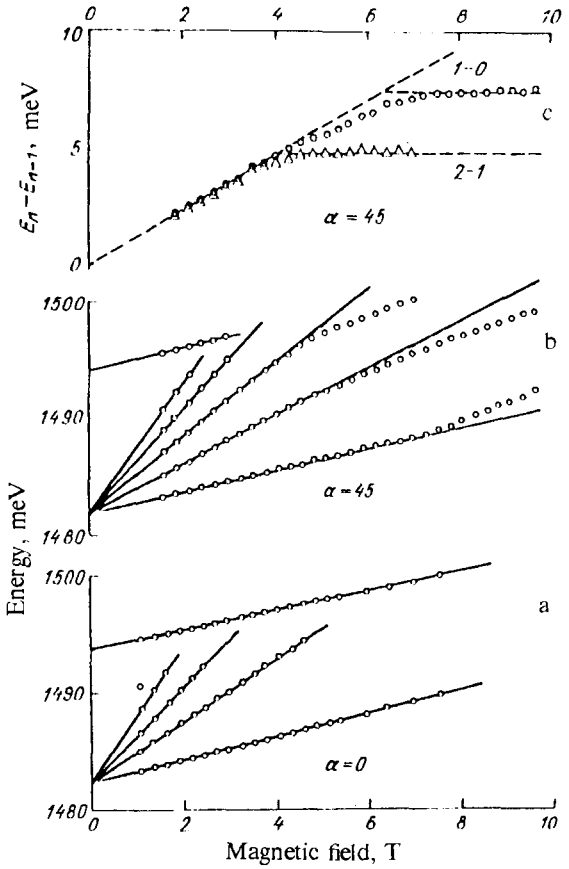

FIG. 8. Position of Landau luminescence peaks in an inclined magnetic field as a function of H for $n_s = 3\times10^{11}$ cm^{-2}; a—$\alpha=0$, b—$\alpha=45°$; c—level splitting as a function of magnetic field for $\alpha=45°$, $H_1^* \sim 4$ T and $H_2^* \sim 7$ T.

to which electrons relax, exist only in the upper spin state of the ground subband. Hence, effective relaxation, i.e., relaxation without spin flip, can occur only for electrons from the upper spin state of the excited subband. On the other hand, relaxation of electrons from the lower spin level is highly suppressed, which is seen experimentally as an increase in magnetoluminescence intensity. When ν becomes smaller than the odd values, vacancies available to relaxation are also found in the lower spin sublevel, and there is a sharp fall in the intensity. Magneto-optic oscillations carry interesting information, not only about the relaxation processes, but also about the states in the spec trum, i.e., single-particle states in IQHE and Coulomb states in FQHE.

3.6. Energy spectrum of 2D electrons in an inclined magnetic field

An inclined field is widely used in experiments with 2D electrons to demonstrate their two-dimensional character,[4] to investigate the influence of spin degrees of freedom on the energy spectrum,[15] and so on.

It is interesting to consider two limiting cases. The limit of weak magnetic fields corresponds to the situation where the magnetic length $l=l_0/\sin^{1/2}\alpha$ determined from the longitudinal component of the magnetic field $H_l=H\sin\alpha$ is much greater than the linear size of the quantum well l_z ($l \gg l_z$). The effect of H on the spectrum of 2D carriers can be taken into account in this limit by perturbation theory. The correction δE_n to the energy E_n of the nth level of dimensional quantization then arises in the second order in H, i.e., $\delta E_n \sim (\hbar\omega_c \sin\alpha)^2 (E_i - E_0)^{-1}$, and the position of the Landau levels changes only because of the anisotropy in the effective mass of the 2D carriers, due to the parallel field. When neighboring Landau levels from different subbands, e.g., the ground and the first excited subbands, are crossed, the magnetic field component lifts the degeneracy because of the repulsion between the levels:

$$\Delta E_{0,1}^{N,N-1} = \frac{|\langle 0|Z|1\rangle|}{\lambda_H \cos^{1/2}\alpha} (2N)^{1/2} \hbar\omega_c \sin\alpha. \qquad (3.4)$$

The significant point here is that, in this limiting case, cyclotron rotation is two-dimensional in character and is entirely determined by the normal component of the field ($\omega_c = eH\cos\alpha/m_c$). The effect of H on the splitting of Landau levels in weak fields was investigated with the help of cyclotron resonance in Refs. 48 and 49.

The other limit, for which $l \ll l_z$ and the fastest motion is the rotational motion of electrons around the direction of the magnetic field with frequency $\omega_c = eH/m_c$, is also interesting and is determined by the total magnetic field H. The particle does not then 'feel' the dimensional quantization and travels classically on a cyloid whose axis points along the field. In this case, the ground-state energy shifts with increasing field more rapidly than in the case of weak fields. On the other hand, motion along the field may be looked upon as adiabatic, and for $H \to \infty$, the low-lying part of the carrier spectrum is determined by the position of the levels in the one-dimensional potential. The splittings of $E_{mn}^*(\alpha)$ between low-lying levels do not depend in this limiting case on the magnetic field, and are much smaller than the original interband splittings of E_{nm}. For example, for the model potential $U(2) \sim Z^\nu$

$$E_{nm}^*(\alpha) = \cos^{2\nu/(\nu+2)}\alpha \cdot E_{nm}, \qquad (3.5)$$

and for the parabolic well[50,51]

$$E_{nm}^*(\alpha) = (n-m)\left\{\frac{1}{2}(\omega_c^2+E_{10}^2) - \left[\frac{1}{4}(\omega_c^2+E_{10}^2)^2 - \omega_c^2 E_{10}^2\cos^2\alpha\right]^{1/2}\right\}^{1/2}$$
$$\sim E_{nm}\cos\alpha. \qquad (3.6)$$

The capacity of each level is determined by the normal field component.

The electron energy spectrum in a strong inclined field ($l \ll l_z$) has been investigated by studying the radiative recombination of 2D electrons with photoexcited holes.[52] Figure 8 shows the position of the energy levels as a function of the magnetic field and the splitting between the levels, determined by analyzing the magnetoluminescence spectra. It is clear that, in a strong inclined field H, the measured relationships depart from straight lines and the splitting between neighboring levels ceases to depend on H.

The residual splitting decreases with increasing angle α. It may be concluded that, beginning $H > H_n^*$, the splitting between the levels E_{mn}^* is determined by dimensional quantization of electrons in the potential well in the direction of the magnetic field. It is important to emphasize that, for a given concentration of 2D electrons, H_n^* is independent of α, whereas for fixed α the field H_n^* decreases significantly with decreasing n_s. We note in conclusion that the measured ratios $E_{10}^*(\alpha)/E_{10}$ and $E_{nm}(\alpha)E_{10}$ as functions of the angle α can be successfully used to determine the shape of the quantum well to which the carriers are confined.

4. MAGNETO-OPTICS OF QUANTUM LIQUIDS IN FQHE

The ground state of an incompressible quantum liquid in the case of the FQHE is described by the trial wave function of a many-electron system proposed by Laughlin[8]:

$$\psi = \prod_{j<k} f(Z_j - Z_k)\exp\left(-\frac{1}{4l_0^2}\sum_i |Z_i|^2\right), \qquad f(Z) = Z^q. \tag{4.1}$$

Although an exact analytic solution of this problem has not yet been found, the wave function (4.1) has been entirely successful. The starting point for Laughlin's idea of the incompressible quantum liquid was Ref. 53. The exponential factor in (4.1) follows from the eigenfunctions of the bottom Landau level, which are classified in accordance with the projections of the angular momentum m (Ref. 54):

$$\psi_m = (2\pi l_0^2 \cdot 2^m m!)^{-1/2}\left(\frac{Z}{l_0}\right)^m \exp\left(-\frac{|Z|^2}{4l_0^2}\right). \tag{4.2}$$

The pre-exponential factor is taken in the Jastrow form, i.e., a product of pair functions. The power form of f follows from (4.2) because only a polynomial that is homogeneous in Z can be an angular momentum eigenfunction. This property guarantees that ψ belongs to the ground Landau level. The degree of the polynomial is determined by the total angular momentum which is a good quantum number, so that m is an odd integer. Next, by analyzing this problem in terms of the single-component classical plasma, Laughlin demonstrated that the wave functions given by (4.1) describe the ground state for $\nu = 1/m$ where $m = q$ is an odd integer. The odd denominator rule of Laughlin's theory is thus seen to follow from the antisymmetry of the many-electron wave function constructed for electrons with the same spin projection. The quantum-liquid wave function can in principle be a singlet, but its exact form is still not known.

For $T = 0$ and $H = \text{const}$, the ground-state energy $E(N)$ of the interacting electrons, where N is the total number of the particles, exhibits a series of cusps for values of N corresponding to fractional filling factors $n = 1/q$. A cusp on the $E(N)$ curve signifies that there is a discontinuous change in the chemical potential $\mu \equiv dE/dN$ as N passes through values N_q corresponding to filling factors $n = 1/q$. This in turn shows that there is a gap in the spectrum, given by

$$\Delta = (dE/dN)_- - (dE/dN)_+ . \tag{4.3}$$

The Coulomb gap separates the ground state of the quantum liquid at the point N_q from the continuum of quasiparticle excitations. The variation in N near N_q produces elementary excitations, i.e., quasiparticles with charges $-e/q$ for $N > N_q$ and quasiholes with charges $+e/q$ for $N < N_q$. It is clear that this picture has nothing in common with the usual elastic compression (expansion) of the electron phase, e.g., the usual Fermi liquid. This means that, in this particular case, the quantum liquid is incompressible for fractional ν, and gapless (acoustic) excitations are absent from its spectrum.

The Coulomb gap is given by $\Delta = Ce^2/\varepsilon l_0$ where C is a constant calculated in different model approximations in Refs. 9 and 55–58. It is commonly considered that the best of these calculations is based on the Monte Carlo method. They show that $C \approx 0.1$ (Ref. 58). A particular Coulomb gap thus corresponds to the creation of a pair of excitations above the gap at infinite distance from one another. In principle, bound (quasiexcitonic) pairs can also be excited. Such excitations should have their own eigenvalue spectra. The spectrum of these excitations contains a roton minimum, in direct analogy with the spectrum of excitations of superfluid He^4. Theoretical calculations[57] show that the roton minimum lies at transferred momenta $kl_0 \approx 1.4$.

The states of quantum liquids in the fractional QHE regime obey the rules of the hierarchy of states. Haldane has proposed a hierarchical scheme[18] in which states p/q with $1 < p < q$, where p is an integer, are formed from new generations of quasiparticle excitations in much the same way that the Laughlin ground state (4.1) is formed from electrons. Daughter states of quantum liquids thus arise from the condensation of quasiparticle excitations of the original 'parent' states. The size of the Coulomb gaps for states with different $1/q$ should be described by the scaling relation (1.3).

It is thus clear that Coulomb gaps determined experimentally in the fractional QHE regime are essential for comparisons with existing theoretical ideas and their further development.

For a long time, activated magnetotransport[59–63] was the only way of measuring Coulomb gaps. This was essentially the method used to measure the mobility gaps in FQHE, which are very sensitive to disorder. At very low temperatures ($T < 1K$), this method encounters difficulties associated with hopping conductivity with variable hop length, and also strong localization effects. It is quite clear that there is a need for an independent method of measuring Coulomb gaps. We shall therefore examine whether the magneto-optic method can be used to solve this problem.

4.1. The properties of magnetoluminescence spectra for fractional ν

Optical experiments with 2D electrons in the fractional QHE regime were first performed with Si–MIS structures.[64] They revealed discontinuous luminescence-line behavior along the energy scale at fractional values $\nu = 8/3$, $7/3$. The magnitude of these discontinuities was

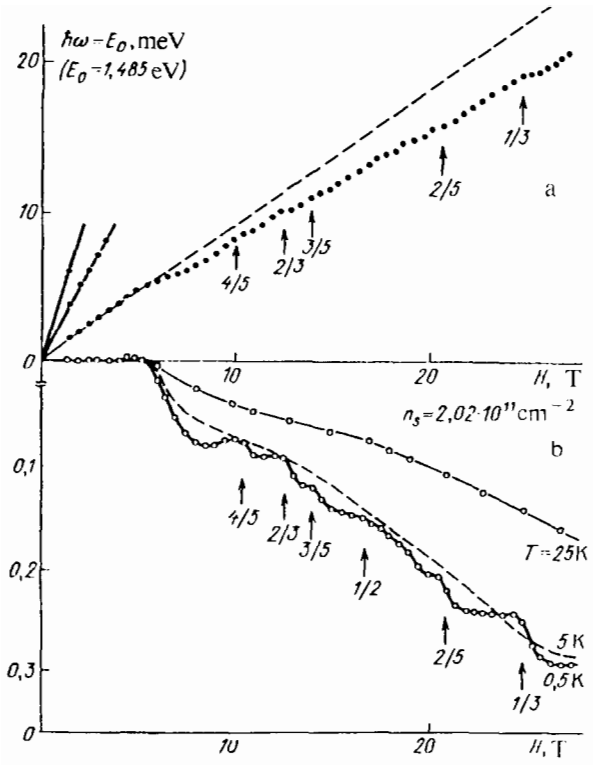

FIG. 9. a—Energy position of a luminescence peak to the recombination of an electron from the lower spin state as a function of the magnetic field H (energy measured from the bottom of the dimensional quantization band; $T=0.47$ K, $n_s=2.02\times10^{11}$ cm^{-2}). b—Energy position of the luminescence peak relative to the dotted line in a as a function of H. Arrows show fractional fillings.

used to estimate the corresponding Coulomb gaps. However, in the case of the 2D electron gas in Si–MIS structures at low temperatures and strong magnetic fields, radiative recombination from the lower spin state $S_z=-1/2$ is not observed because of selection rules, and there are fundamental reasons that prevent observations by magneto-optic methods in the ultraquantum limit. No such limitations arise in the case of the GaAlAs–GaAs heterojunctions because the electron g-factor is negative.

In this Section, we examine magneto-optic measurements on single GaAlAs–GaAs heterojunctions at fractional filling factors $\nu=2/3$, 1/3, 4/5, 3/5, 2/5, 1/5, 1/7, and 1/9 for which the discontinuous behavior of the magnetoluminescence line was also observed.[21] These studies employed high-grade samples in which the 2D electron mobility under illumination was $\mu_e\geqslant10^6-3\times10^6$ $s^2V^{-1}s^{-1}$ and the electron density could be varied by the means of a suitably chosen steady illumination in the range $0.5\times10^{11}-2\times10^{11}$ cm^{-2}.

Figure 9 shows the Landau line peaks in the magnetoluminescence spectrum, obtained by varying the magnetic field. For filling factors $\nu>2$, the picture takes the usual form of fan of Landau levels. However, for $\nu<2$, when only one line remains in the spectrum, new features are found to arise. The maximum deviation from the straight line occurs in the region between $\nu=2$ and $\nu=1$. These deviations are due to enhanced spin splitting that results from the exchange interaction between electrons with the same spin projections (enhanced g-factor). Further increase in the magnetic field results in additional jumps in the spectral position of the center of gravity of the line $\hbar\bar{\omega}$ near $\nu=4/5$, 2/3, 3/5, 2/5, and 1/3. The amplitude of these jumps increases with decreasing temperature. The size of the jumps is small in comparison with the basic energy scale in the spectrum, which is determined by the cyclotron energy. The same results are shown in Fig. 9b after subtraction of the single-electron contribution due to the energy of the bottom Landau level. This makes the jumps in $\hbar\bar{\omega}$ at $\nu=4/5$, 2/3, 3/5, 2/5 and 1/3 more clearly defined. It is interesting to note that a small line broadening (about 10%) is observed near $\nu=p/q$. However, this does not affect the line shape. There is also a relatively broad singularity near $\nu=1/2$. When the temperature is raised to 5 K, all the jumps corresponding to filling factors with odd q are found to vanish, but the $\nu=1/2$ singularity persists up to 25 K. The slight temperature sensitivity of this singularity is similar to that observed in magnetotransport.[65,66] In particular, magnetotransport studies[66] show that the $\nu=3/2$, 3/4, 1/2, and 1/4 singularities have a common origin that is unrelated to FQHE.

The dependence of ΔE on H becomes more negative as the temperature is reduced, which is associated with strong localization in the magnetic field. This can be used for the analysis of disorder in the system.

By using a series of samples with decreasing concentration of 2D electrons, it is possible to move deeper into the ultraquantum region ($\nu\ll1$). The discontinuous behavior of the center of gravity of the luminescence line for $\nu=2/3$, 1/3, 4/5, 3/5, 2/5, 1/5, 1/7, and 1/9 is illustrated in Fig. 10. These results are fully reproduced after thermal cycling. We note that similarly well-defined singularities at $\nu=1/7$ and 1/9 in FQHE were found for the first time, but magnetotransport measurements did not reveal the singularity at $\nu=1/9$. This clearly shows that, in comparison with magnetotransport, strong localization effects are much less effective in restricting the magneto-optic method. Figure 10 compares the functions $\Delta E(H)$ measured at three different temperatures. At 0.4 K, the behavior of the function is discontinuous for all observed fractions $\nu=1/q$ up to 1/9, but no features are observed near 1/11. At $T=1.2$ K, the jumps at $\nu=1/7$ and 1/9 vanish; however, they persist for other fractional $\nu=p/q$ with smaller q.

Finally, we turn to the very topical problem of the true electron temperature in the above experiments under steady photoexcitation. The problem was solved by analyzing the linewidths of Shubnikov oscillations in longitudinal magnetoresistance, which acted as an external electron thermometer. The longitudinal resistance was measured simultaneously (*in situ*) with magneto-optic properties. For example, under stationary photoexcitation by an argon laser with a power output of about 1 MW and with a bath temperature of 40 mK, the electron temperature was found to rise, but did not exceed 100 mK. It follows that these structures can be used to perform magneto-optic studies at temperatures much less than 1 K because of the much

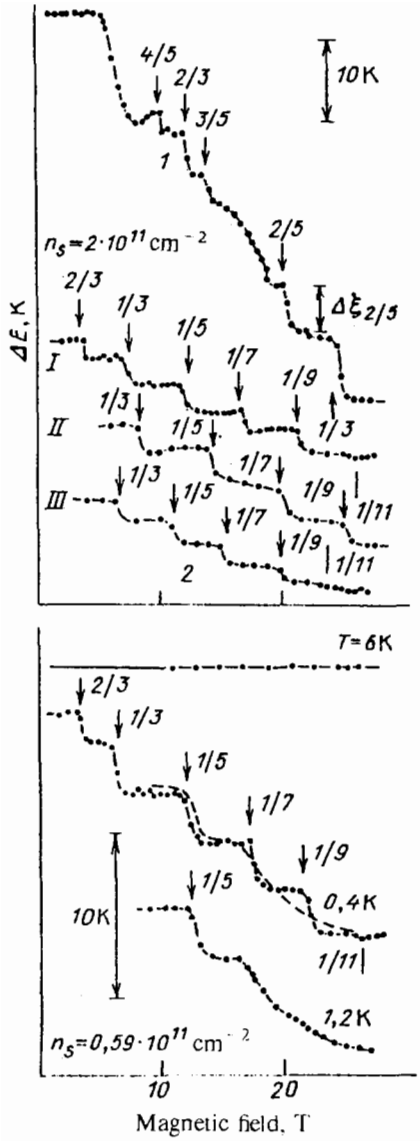

FIG. 10. Center of gravity $\bar{\omega}$ of the luminescence line due to the recombination of an electron for the lower spin state as a function of the magnetic field. $\Delta E=\hbar\bar{\omega}-(1/2)\hbar\omega_c$.

longer time constants for radiative recombination of 2D electrons in these systems.

4.2. Theory of magnetoluminescence from 2D electrons in FQHE

We now turn to the interpretation of the above experimental results. It was believed in early discussions[64] of the discontinuous behavior of the center of gravity of the Si–MIS magnetoluminescence line at fractional filling factors that this behavior was directly related to discontinuities in the chemical potential when the 2D electrons condensed into the Laughlin quantum liquid: $\Delta\bar{\omega}=\Delta\mu=q\Delta_q$. The spectral jump $\Delta\bar{\omega}$ could then be directly used to determine the Coulomb gap corresponding to a given fraction $1/q$. This hypothesis was based on the assumption that the initial state of the N electrons prior to recombination and the final state of the $N-1$ electrons after recombination were both ground states. In other words, the interacting system of 2D electrons was assumed to follow adiabatically the radiative recombination with the acceptor center. This was an attractive hypothesis because the recombination event in the interacting system of $N-1$ electrons was followed by the appearance of different excitations whose subsequent relaxation to the ground state after this shake-up process required a sufficient interval of time.

A theory[67] capable of analyzing the radiative recombination of an interacting system of 2D electrons with holes in an acceptor center has recently been reported. The analysis is concerned with the behavior of the first moment M_1 of the luminescence line when the filling factor is varied near a fractional value of ν:

$$M_1\equiv\int I(E)E\mathrm{d}E/\int I(E)\mathrm{d}E$$

coincides directly with the center of gravity of the line $\bar{\omega}$. The main result is that $M_1(\nu)$ reflects the behavior of the mean energy of the interacting electrons and not the chemical potential.

The theory is based on the following model assumptions. The electron density is assumed to be homogeneous and the acceptor center originally neutral. The separation Z_0 between the impurity center and the 2D plane, and the magnetic length l_0, are much greater than the width of the electron layer and the radius of the impurity center (Z_0, $l_0\gg r_{\mathrm{imp}}$). In the final state, the potential of the impurity center is a repulsive Coulomb potential. At $T=0$, the electron system is in the ground ith state; when this state is degenerate, it is assumed that all the states are equally filled. The magnetic field is assumed to be so strong that $\hbar\omega_c\gg e^2/\varepsilon l_0$, and mixing of the different Landau levels can be neglected. In other words, the mixing parameter for the Landau levels $\lambda=(e^2/\varepsilon a)/\hbar\omega_c\equiv(1/2\nu)r_s$ is assumed to be zero [$a=(\pi n_s)^{-1/2}$ is the particle separation, $r_s=a/a_B$, and $a_B=\varepsilon\hbar/me^2$ is the Bohr radius]. This is equivalent to the situation for which $r_s\to0$. The radiative quantum transition occurs at the point r_0 in the 2D layer that is closest to the impurity center. The calculations are performed numerically in spherical geometry.[68,69] All the equations are thus written down for the homogeneous system with a finite number of particles (in practice six and seven particles).

The normalized first moment of the magnetoluminescence line is thus given by

$$M_1=E_i-\langle H_f\rangle_{ab}. \tag{4.4}$$

where E_i is the ground-state energy of the N interacting particles and H_f is the Hamiltonian of the system in the final state, i.e., the energy of the $N-1$ electrons with coordinates $\mathbf{r}_1...,\mathbf{r}_{N-1}$ in the 2D layer, which interact with one another and with a repulsive Coulomb center at $\mathbf{r}_i$. The average in (4.4) is evaluated over wave functions $\psi_\alpha(\mathbf{r}_1,...\mathbf{r}_N)$ of all states α belonging to the ith level, subject to the condition $\mathbf{r}_N=\mathbf{r}_0$. After subtraction of the energies of the ground Landau level and the impurity center, the first-order moment of the center of gravity of the magnetolu-

minescence line contains only the energy of the Coulomb interaction between the particles. Equation (4.4) then assumes the form

$$M_1=\int\left(V(|\vec{\rho}_0-\vec{\rho}|)-V(|\vec{\rho}_1-\vec{\rho}_0|)g(|\vec{\rho}_0-\vec{\rho}|)\mathrm{d}\vec{\rho}\right.$$

$$=2E_iN^{-1}-\int V(|\vec{\rho}_1-\vec{\rho}|)g(|\vec{\rho}_0-\vec{\rho}|)\mathrm{d}\vec{\rho}. \quad (4.5)$$

The integral in this expression is evaluated over the entire 2D layer, and the pair correlation function is given by

$$g(|\vec{\rho}_N-\vec{\rho}_{N-1}|)$$

$$=\frac{1}{g_i}(N-1)Al_0^2\sum_\alpha\int|\psi_\alpha(\mathbf{r}_1\cdots\mathbf{r}_N)|^2\mathrm{d}\mathbf{r}_1\cdots\mathrm{d}\mathbf{r}_{N-2}, \quad (4.6)$$

$$\int g(\vec{\rho})\mathrm{d}\vec{\rho}=N-1,$$

where g_i is the degeneracy of the ith level, A is the area of the 2D layer, and $\vec{\rho}=\mathbf{r}/e$.

If $V(\mathbf{r})$ is a short-range potential, the second term in (4.5) can be simply discarded. If we use the definition of the chemical potential in the form $\nu=\partial E_i/\partial N$ then (4.5) readily yields the following expression for the Coulomb gap:

$$\Delta_q=(\nu/2q)\delta(\partial\bar{\omega}/\partial\nu)\equiv(H/2q)\delta(\partial\bar{\omega}/\partial H). \quad (4.7)$$

Hence the line center of gravity function $\bar{\omega}(\nu)$ follows the mean energy of the Coulomb interaction between the particles and displays cusps for fractional ν. The cusp strength, defined as the discontinuity in the derivative $\partial\bar{\omega},/\partial d\nu$, can be used to deduce the gap size Δ_q.

However, $V(r)$ is actually a long-range Coulomb potential and, in principle, the second term in (4.5) has to be taken into account. It is interesting to note, that as $Z\to 0$, we have $\bar{\omega}=0$. This means that, if the 2D electrons in the impurity center (or free hole) are coplanar, the two terms in (4.5) cancel out, and there are no singularities in $\bar{\omega}(\nu)$ near fractional ν.

For finite Z_0, the extrinsic contribution to the cusp strength in $\bar{\omega}(\nu)$ is not small. The general expression for the cusp strength is

$$\delta\left(\frac{\partial\bar{\omega}}{\partial\nu}\right)=\frac{2q\Delta}{\nu}-\int V(|\vec{\rho}_1-\vec{\rho}|)\delta\left(\frac{\partial g(|\vec{\rho}_0-\vec{\rho}|)}{\partial\nu}\right)\mathrm{d}\vec{\rho}. \quad (4.8)$$

In the expansion for (4.8), the term $\sim Z_0^{-1}$ is absent from the normalization condition for $Z_0\gg l_0$, whereas for $Z_0\ll l_0$ the expansion is proportional to Z_0^2.

The pair correlation function can be used to calculate the second (extrinsic) term in (4.8) as a function of h and the results are as follows:

$$\delta(\partial\bar{\omega}/\partial\nu)\approx 18\Delta-37\varepsilon(l/Z_0)^3 \quad \text{for } Z_0\gg l,$$

$$\approx 0.77(Z_0/l)^2 \quad \text{for } Z_0\ll l. \quad (4.9)$$

Hence it follows that the exintrinsic contribution to the general expression for the cusp strength rapidly decreases with increasing distance Z_0 of the impurity center from the 2D plane. This means that, for sufficiently large distances Z_0, the procedure that has to be used to analyse the experimental data on $M_1(\nu)$ in order to determine the gap size becomes much simpler.

4.3. Coulomb gaps in FQHE

Let us now consider how the experimental data on the center of gravity of a luminescence line or its first moment $M_1(\nu)$ were used to determine the gap size in accordance with the theoretical predictions.

The experimental luminescence spectra were analysed by calculating the zeroth (M_0), first (M_1) second (M_2), and third (M_3) spectral moments:[70]

$$M_0=\int I(E)\mathrm{d}E, \quad M_1=\frac{1}{M_0}\int I(E)E\mathrm{d}E,$$

$$M_2^2=\frac{1}{M_0}\int I(E)(E-M_1)^2\mathrm{d}E,$$

$$M_3^2=\frac{1}{M_0M_2^3}\int I(E)(E-M_1)^3\mathrm{d}E.$$

All the experimental data obtained for constant values of the magnetic field were processed on a computer. We recall that M_0, M_1, M_2 and moment M_3 characterizes the integral intensity, the center of gravity, the width, and the asymmetry of a luminescence line. The uncertainty with which the first moment M_1 was determined was less than 0.01 meV. Figure 11a compares the behavior of the function $M_1(H)$ with the picture of Shubnikov oscillations in magnetoresistance for a sample with high mobility[70] (1.2×10^6 cm^{2}V^{-1}s^{-1}). It is clear that the minima of ρ_{xx} coincide with downward cusps of $M_1(H)$. This is more clearly seen in Fig. 11b which compares the four moments M_1, M_2, M_3, M_0 as functions of H with the minimum of ρ_{xx} near $\nu=1/3$. It is clear that the minimum of ρ_{xx} coincides with the cusp of $M_1(H)$ at $\nu=1/3$, so that this function probably reflects the mean energy of 2D electrons rather than its chemical potential. We also note that the upward cusp of $M_1(H)$ lies near the maximum of ρ_{xx}. In many cases, the spectrum of radiative recombination of 2D electrons and an acceptor center was investigated in parallel with spectra corresponding to recombination with free holes. However, no cusps were found on $M_1(\nu)$ for fractional ν.

Figure 12 shows simultaneously recorded data on the Shubnikov oscillations in ρ_{xx}, the first-order moment $M_1(H)$, and its derivative $\mathrm{d}M_1/\mathrm{d}H$ measured for a sample with 2D electron concentration $n_s=2.4\times 10^{11}$ cm^{-2} at $T=100$ mK in the neighborhood of filling factors $\nu=8$, 6, 4, 3, 2, 1 and 2/3 (Ref. 71). The presence of downward cusps on $M_1(H)$ becomes particularly clear if we examine the corresponding discontinuities in the derivative $\mathrm{d}M_1/\mathrm{d}H$. Figure 12 shows the jumps for $\nu=2$, 4, 6, 8, 10 (cyclotron gaps), $\nu=1$, 3, 5, (gaps due to spin splitting), and $\nu=4/5$, 2/3, and 3/5 (Coulomb gaps for fractional ν).

For IQHE, the mean energy of electrons is determined by the shape of their distribution over the Landau levels. Here again we see downward cusps on $M_1(H)$ that appear

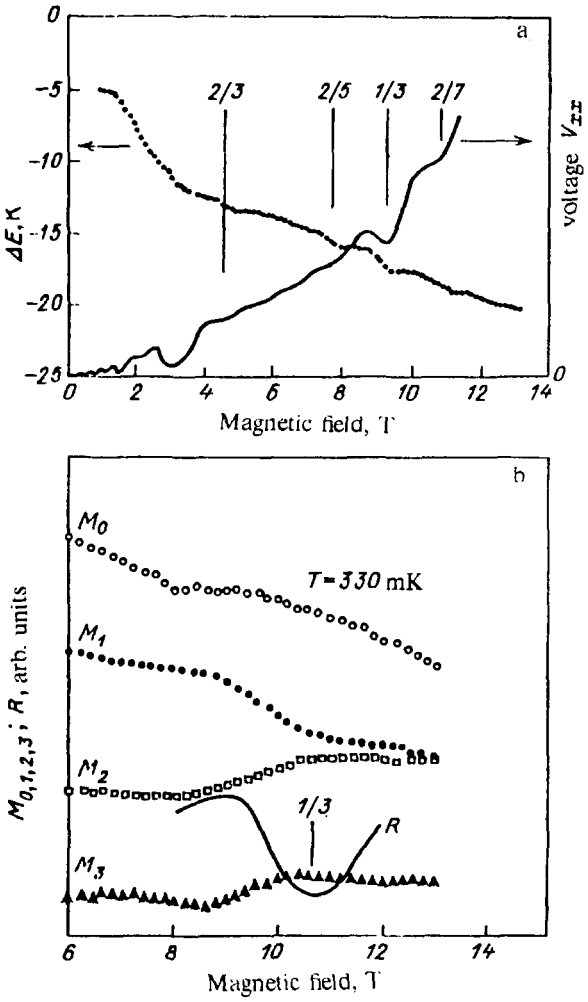

FIG. 11. a—Correspondence between Shubnikov oscillations in magnetoresistance and the moment $M_1(H)$; $T=0.6$ K. b—The moments M_0, M_1, M_2, M_3 of the magnetoluminescence line near $\nu=1/3$. Solid line—magnetoresistance; $T=330$ mK.

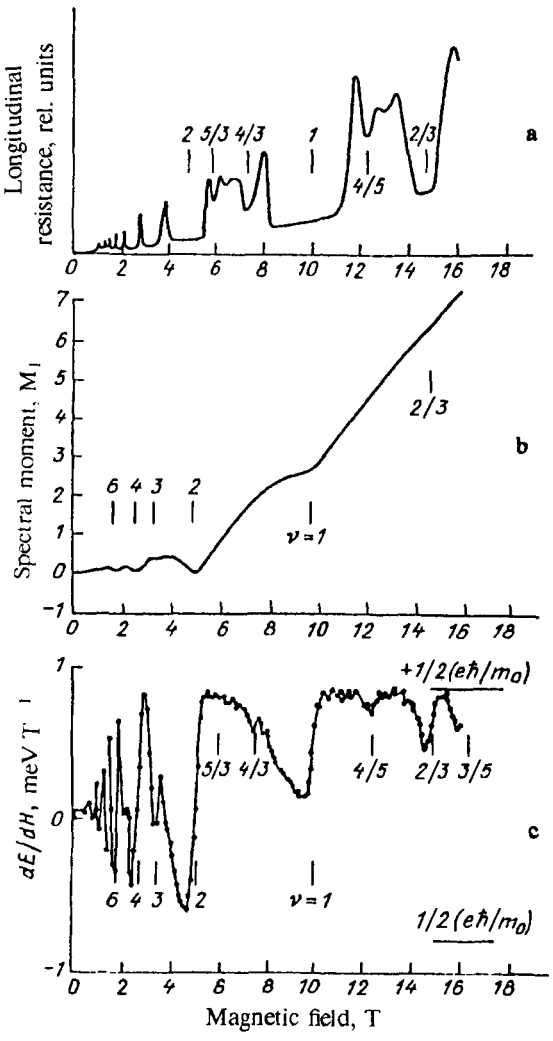

FIG. 12. First moment M_1 (b) and its derivative (c) as functions of magnetic field H compared with the Shubnikov oscillations (a). Integral and fractional fillings are indicated.

for even integral values of ν. These cusps determine the discontinuous behavior of the chemical potential as the Landau levels are crossed. In the case of the ideal picture of discrete Landau levels, one can readily use the jump in the derivative $dM_1/d\nu$ to determine the cyclotron gap if there is no electron-electron interaction and $T=0$. The relevant expression is

$$\Delta_G=\hbar\omega_c=\nu\delta(dM_1/d\nu)=H\delta(dM_1/dH). \qquad (4.10)$$

We now draw attention to the fact that (4.7) and (4.10) are identical apart from the factor of 2. In (4.7), which gives the Coulomb gap in FQHE, this factor is due to the pair character of the e, e interaction.

When $\nu=2$ and the temperature T is low enough, we can readily verify (see Fig. 12) that the jump in dM_1/dH is practically equal to $e\hbar/m_c$ which can be determined independently from the Landau splitting in optical spectra. For high even integral values of ν there are deviations due to the broadening of the Landau levels and the relatively large discrete step in the magnetic field under these experimental conditions.[71] As the temperature increases, the derivative dM_1/dH decreases in amplitude and monotonically broadens in the region of the cyclotron gaps. This temperature evolution of the downward cusp on $M_1(H)$ and the derivative $dM_1/(H)/dH$ is not at all surprising and is a consequence of the Fermi distribution function.

The jumps on $dM_1(H)/dH$ in Fig. 12 are associated with spin splitting for $\nu=1$ and Coulomb gaps in FQHE for $\nu=4/5$, 2/3, and 3/5. The derivative dM_1/dH was calculated numerically from the directly measured $M_1(H)$.

The Coulomb gaps and their dependence on the magnetic field, determined by this procedure, are illustrated in Fig. 13 for $\nu=p/3, p/5, p/7$ and 1/9. The circles represent Δ_q determined directly from the size of the discontinuity in the derivative $dM_1(\nu)/d\nu$, using the approximate formula given by (4.7). The crosses show the same gaps after correction by the procedure described in Ref. 67, taking into account the finite distance Z_0 between acceptors and the interface. The experimental values are compared with the theoretical dependence of Δ_q on H (Refs. 58 and 72), which is represented by the solid lines. The dashed lines show the approximation giving the best agreement with

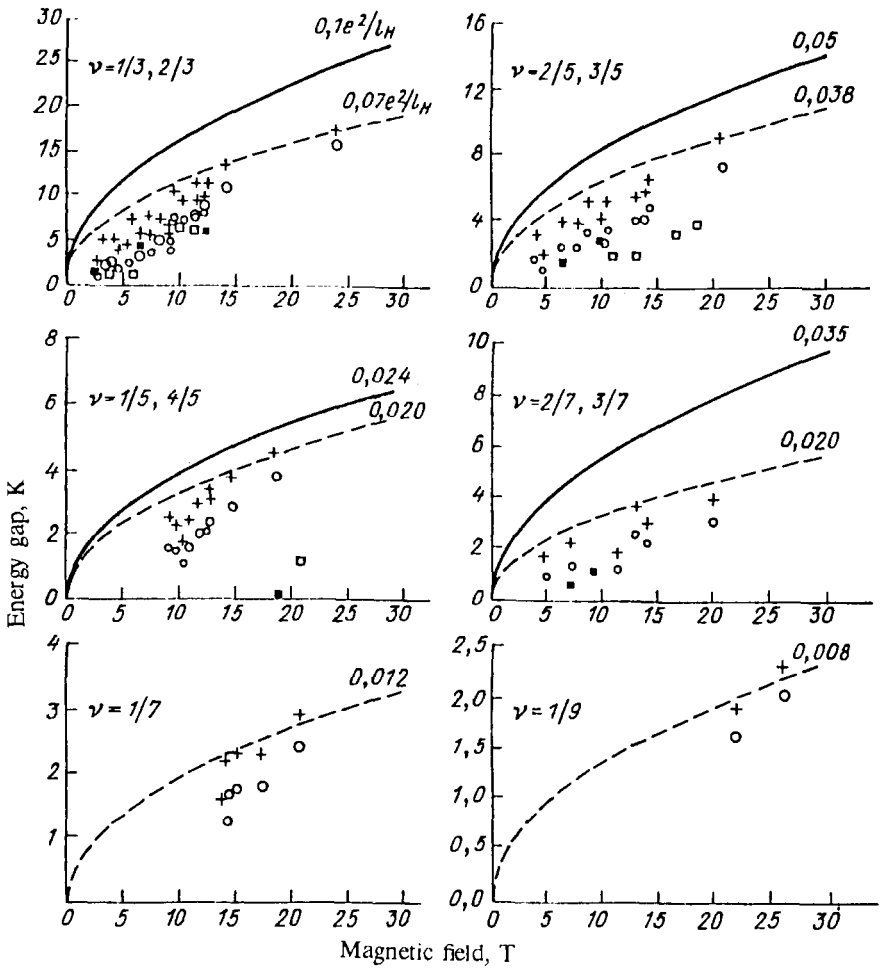

FIG. 13. Coulomb gaps of QL in fractional QHE as functions of magnetic field. See text for explanation of symbols.

experiment. We recall that theoretical calculations indicate that the Coulomb gaps are reduced in size when the finite width of the 2D electron channel and the mixing of the Landau levels are taken into account.[73] Finally, for the purposes of comparison, we also reproduce the data obtained by activated magnetotransport (filled and open squares represent data from Refs. 62 and 63). The agreement between optical and transport measurements is best—and completely satisfactory—for $H > 10$ T, but the data show a considerable discrepancy for lower values of H. The reason for this discrepancy is probably the fact that the magnetotransport measurements yield the mobility gaps. When the mobility gap is comparable with the Landau level width, magnetotransport results in a considerable underestimate of the true gap width.

The temperature dependence of a Coulomb gap is not a trivial result. Figure 14a shows the derivative $dM_1(H)/dH$ at $\nu=2/3$ and 3/5 at different temperatures. The jump in the derivative is practically constant up to a certain temperature. For fundamental reasons, this effect cannot be detected by means of activated magnetotransport. Figure 14b shows the Coulomb gap energies for $\nu=2/3$, 3/5, 1/5, and 1/7, determined from $\delta(dM_1(H)/dH)$ by the procedure described above. It is clear that each fraction has its own characteristic temperature T_c after which the corresponding gap collapses. Similar behavior had been observed earlier for FQHE in Si-

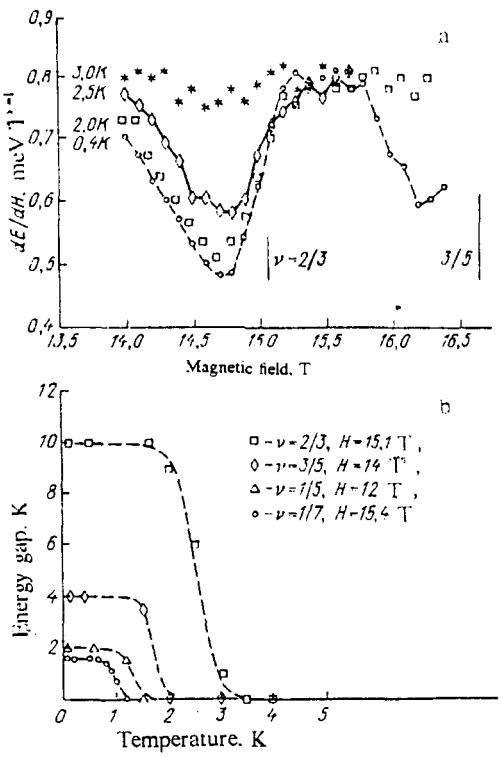

FIG. 14. (a)—Cusp strength dM_1/dH as a function of temperature. (b)—Temperature dependence of Coulomb gaps for $\nu=2/3$, 3/5, 1/5, 1/7.

MIS structures. The thermal collapse is also observed in the case of spin splitting ($\nu=1$). There is a simple empirical relation between the gap size $\Delta(T=0)$ and the critical temperature. To explain this effect in the case of the FQHE it would probably be necessary to take into account the total dispersion of the spectrum of quasiparticle excitations, including its roton part.

4.4. Magneto-optic experiments in FQHE for other heterosystems

The magnetoluminescence of 2D electrons and free holes in a high-grade single GaAlAs–GaAs heterojunctions was investigated in Refs. 74 and 75 (the mobility of the 2D electrons in these structures under illumination was of the order of 10^7 $cm^2V^{-1}s^{-1}$). A study was made of oscillations in intensity due to recombinations of 2D electrons from the ground (E_0 line) and excited (E_1 line) subbands of dimensional quantization as a function of magnetic field. It was found that the E_0-line minima and the E_1-line maxima of magnetoluminescence intensity corresponded to integral ν for IQHE and to fractional ν for FQHE. This oscillatory behavior is explained in terms of the screening by electrons of photoexcited free holes, and also the incompressability of the Fermi liquid. The oscillations are undoubtedly indicators of highly correlated electron states in FQHE. However, the oscillation can hardly be used for the measurement of the size of Coulomb gaps.

The radiative recombination of 2D electrons with free holes in doped asymmetric single GaAlAs–GaAs quantum wells was investigated in Ref. 76. These experiments revealed the splitting of luminescence lines near $\nu=2/3$, which was not directly related to the corresponding Coulomb gap; the nature of the splitting is not as yet entirely clear.

Finally, there have been some very interesting experiments on resonant electron scattering of light by 2D electrons.[77] Inelastic scattering of light was detected in these spectra and was related to energy transfers to the roton minimum in the spectrum of quasiparticle excitations. If these observations and, especially, their interpretation, can be confirmed, the resonant scattering of light by 2D electrons may turn out to be one further optical tool for the determination of the spectrum of Coulomb gaps in FQHE.

5. MAGNETO-OPTIC OBSERVATIONS OF CRYSTALLIZATION OF 2D ELECTRONS

In this Section, we consider the interesting problem of how the crystallization of 2D electrons in the ultraquantum limit can be observed by magneto-optic methods. We shall be mostly interested in the competition between the ground states of quantum liquids in FQHE and the Wigner crystal, and in the effect of this competition on the phase diagram of the crystal to liquid transition.

5.1. Theoretical aspects of the problem

Almost sixty years ago, Wigner predicted[78] that, when the Coulomb interaction energy $\langle V\rangle$ is much greater than the kinetic energy $\langle K\rangle$, a set of electrons should form a stable configuration with long-range order. In the free-dimensional case, the lattice with the lowest internal energy is the body-centered cubic, whereas in the two-dimensional case, it is a hexagonal lattice.

For 2D electrons in zero magnetic fields, it is common to distinguish between classical and quantum limits in which this type of crystallization can take place. The classical case (or the low-density region) is defined by the inequalities $\hbar^2/m^*a^2 \ll kT \ll e^2/\varepsilon a$ where m^* is the effective mass of the electron and a is the separation between the particles. In this limit, the phase transition from the liquid to the electron 2D crystal occurs for $\langle V\rangle/\langle K\rangle = e^2(\pi n_s)^{1/2}/\varepsilon kT > \geqslant \Gamma \approx 10^2$. It is precisely this type of crystallization of 2D electrons in the classical approximation that was detected and investigated in experiments with electrons on the surface of He (Refs. 79 and 80). These studies have resulted in the determination of the transition phase boundary on the n_s, T_c plane, the classical melting point $T_c = e^2(\pi n_s)^{1/2}/\Gamma_m \varepsilon k$, and the magnitude of the parameter Γ_m.

The quantum limit (or the region of high concentrations) occurs when $kT \ll \hbar^2/m^*a^2 \ll e^2/\varepsilon a$. In this region, the ratio $\langle V\rangle/\langle K\rangle$ is analysed as a function of the dimensionless parameter $r_s \equiv a/a_B$. Since the correlation energy is $\langle V\rangle \sim n_s^{1/2}$ and the kinetic energy is $\langle K\rangle \sim n_s$, the Wigner 2D crystal is stable for $r_s > \Gamma_W$, i.e., when the electron density does not exceed a certain limiting value defined by $n_s \leqslant n_W = (\Gamma_W^2 \pi a_B^2)^{-1}$. In this situation, the phase diagram has an end-point on the concentration axis. Numerical calculations show[81] that $\Gamma_W \approx 33$. If we adopt this value of Γ_W, we find that quantum crystallization of 2D electrons occurs on the surface of helium for $n_W \approx 10^{13}$ cm^{-2} whereas the corresponding figure for 2D electrons in a GaAlAs–GaAs heterojunction is $n_W \approx 10^8$ cm^{-2}. These conditions cannot be met in such systems, which has meant that Wigner crystallization of 2D electrons has not been observed in the quantum regime in the absence of a magnetic field.

The situation is radically different when a strong transverse magnetic field is applied. The electrons then lose their previous degrees of freedom and execute finite motion on cyclotron orbits with dimensions $(2N+1)^{1/2}l_0$. In the quantum limit ($\nu<1$), the correlation interaction ensures that the mean energy of the 2D electrons is reduced without any loss in kinetic energy. A strong magnetic field thus establishes favorable conditions for the spatial ordering of electrons, i.e., it stimulates Wigner crystallization.

We have to know the critical filling factors ν_c above which the crystalline phase of electrons becomes energetically more favorable than the quantum liquid in FQHE before we can carry out experiments in the quantum limit. The phase boundary between the Wigner crystal and the liquid can be fully described by using three parameters, namely, the filling factor ν, the dimensionless density r_s, and the dimensionless temperature $\Gamma = kT/(e^2/\varepsilon a)$. In the three-dimensional space (ν,Γ,r_s), the transition phase diagram should take the form of a topologically complex surface. For high densities, r_s may be looked upon as the

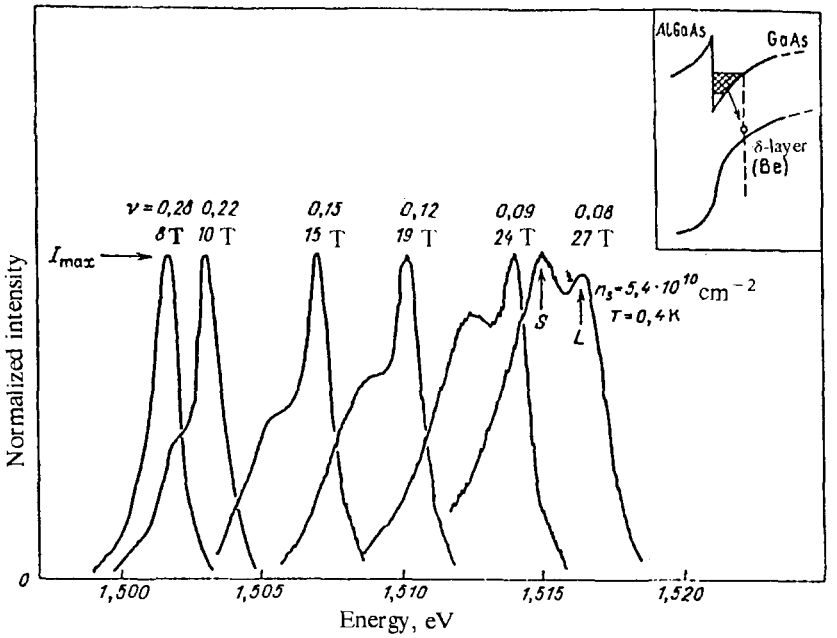

FIG. 15. The spectra of 2D electrons recombining with photoexcited holes in an acceptor monolayer, recorded in different magnetic fields ($n_s = 5.4 \times 10^{10}$ cm^{-2}, $T = 400$ mK). The spectra are normalized to the same intensity.

equivalent of λ which characterizes the mixing of Landau levels $\lambda = (e^2/\varepsilon a)/\hbar\omega_c = \nu r_s/2$. Most microscopic calculations of the ground-state energy of the Wigner crystal are concerned with the limit $r_s \to 0$. They yield values of ν_s between 1/5 and 1/10 (Refs. 30 and 82). Correlation effects in the case of mixing between Landau levels are taken into account in Refs. 83 and 84 where it is shown that there is an associated increase in the stability of the Wigner crystal. The most stable crystal phase occurs for $\nu_c = 1/3$. For example, $r_s \approx 20$ for the hole-type 2D channel in GaAlAs–GaAs.

A reduction in the dimensionality of the system results in new properties of the 2D crystal and in singularities in the transition from the liquid to the 2D crystal as compared with ordinary three-dimensional objects. The properties of the 2D crystal were first examined by Peierls who showed that the amplitude of zero-point oscillations, or the root mean square deviation of a particle from its equilibrium position in the lattice, increases logarithmically with the size of the system at any finite temperature. This means that the 2D crystal with unlimited dimensions is unstable. The problem can be solved in two different ways.

First, numerical model calculations show that the stability of the two-dimensional crystal is greater when it is split into domains, and that the smaller the size of the 2D domain, the higher its melting point.[85]

Another approach was developed by Kosterlitz and Thouless[86] (see also the review in Ref. 87). They showed that long-range order cannot occur in the 2D case in the ordinary sense, but that it is possible to introduce a criterion that will distinguish between liquid and crystal phases. In particular, in the liquid case, positional order vanishes exponentially, whereas in the two-dimensional crystal this occurs much more slowly, i.e., the loss of order is described by a power function of distance. In contrast to the ordinary three-dimensional liquid-to-crystal transition, which is a first order transition with a particular latent heat, theory predicts a continuous transition from the low-temperature phase with quasi-long-range positional order to the high-temperature disordered phase. The transition itself is characterized by singularities in energy and heat capacity.

Nelson and Halperin have suggested[88] that the melting of the 2D crystal is the result of the dissociation of structural defects, namely, dislocation pairs. The phase transition itself occurs in two stages and is characterized by two critical points, namely, T_{c1} for the transition between the 2D crystal and the hexatonic liquid with orientational order (the so-called hexatonic phase) and T_{c2} above which the orientational order is lost in the liquid phase.

One of the most suitable objects for the investigation of 2D electrons in a strong magnetic field in Wigner crystallization is the single GaAlAs–GaAs heterojunction. Improved technologies can be used to produce in such structures two-dimensional channels with electron mobilities of 10^6–10^7 cm^{2}V^{-1}s^{-1} for 2D carrier concentrations $n_s = 10^{10}$–10^{11} cm^{-2}. Recent experiments that are conceptually and methodologically different have examined radiofrequency absorption,[17,89] nonlinear magnetotransport,[19,89–91,96] the attenuation of surface acoustic waves,[92] cyclotron resonance,[93] and magneto-optics.[21,75] They have produced substantial evidence for the fact that this crystallization does occur. Its manifestations in magneto-optic experiments are examined below.

5.2. Luminescence spectrum in Wigner crystallization

It was found in Ref. 21 that the spectrum of radiative recombination between 2D electrons and holes in a δ-layer of acceptors in a single GaAlAs–GaAs heterojunction contains a new line (the so-called S-line) for $\nu < \nu_c$ and $T < T_c$. The relative intensity of the S-line increases with decreasing filling factor.

Figure 15 shows the normalized luminescence spectra obtained in different magnetic fields for a particular sample in which the 2D electron concentration under stationary illumination was $n_s = 5.4 \times 10^4$ cm^{-2}. In addition to the

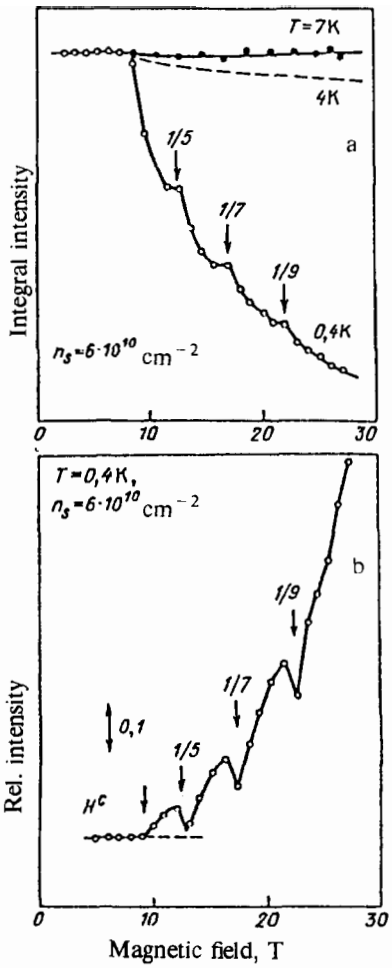

FIG. 16. The integral luminescence intensity (a) and S/L intensity ratio at $T=600$ mK as functions of magnetic field.

well-known L-line that corresponds to the recombination of electrons from the lower spin state in the liquid phase, the spectrum now contains the new S-line that appears when certain particular values of the magnetic field are reached. The line becomes stronger with increasing H, and dominates the spectrum for $\nu\approx 0$ and 1. The S-line is shifted toward lower energies, and the splitting between the S and L lines amounts to 1.4 meV. It is significant that the appearance of the S-line in the spectrum is accompanied by the beginning of a rapid reduction in the integral luminescence intensity in this region. This is illustrated in Fig. 16 which shows the integral luminescence intensity and the S/L intensity ratio as functions of the magnetic field H. The fall in the integral intensity and the rise in the S-line intensity occur for the same magnetic field H_k. Measurements on samples with different concentrations n_s have shown that H_k increases linearly with increasing n_s.

The phenomena described above for this particular range of concentrations are thus found to be independent of n_s and are observed for filling factors $\nu<\nu_k=0.26$. It is important to note that the S-line intensity decreases sharply near $\nu=1/5$, 1/7, and 1/9 for which condensation into the quantum liquid takes place. At the same time, the integral luminescence is found to rise due to the increase in the L-line intensity for the same fractional filling factors.

The S-line is very sensitive to temperature. It vanishes from the spectrum for $T>1.4$ K and $H=26$ T. This is accompanied by an increase in the integral luminescence intensity and a return to the initial values for $H<H_k$. The critical temperature is very dependent on the filling factor: for $\nu<\nu_k$ it increases with decreasing ν, but it falls sharply for $\nu=1/5$, 1/7, and 1/9.

The appearance of the new S-line in the spectra, which is accompanied by the simultaneous sharp reduction in the integral luminescence signal, is due to the emergence of the crystal phase in the system of interacting electrons. In this interpretation, the S and L lines correspond to the radiative recombination of 2D electrons from the crystal and liquid phases, respectively (quantum Fermi liquids for $\nu=1/5$, 1/7, and 1/9). The shift of the S-line toward lower energies as compared with the L-line signifies that the ground state of the crystal phase is the lowest state. The vanishing of the S-line for $\nu=1/5$, 1/7, and 1/9 indicates that, for such fractional fillings, the ground state of the system is still the quantum liquid. The sharp reduction in the integral luminescence signal is a consequence of the strong localization of electrons under crystallization conditions. Actually, the size of the electron and hole wave functions participating in recombination is determined by the magnetic length in the 2D plane. On the other hand, the magnetic field has little effect on the wave functions of the recombining particles in the perpendicular direction. It is clear that the overlap of the wave functions of the highly localized electrons and holes decreases with increasing H. The localization of electrons is intrinsic in this case. This follows from the fact that a qualitative change in structure does not affect the critical filling factor ν_c. The observed phenomenon is due to the appearance of the 2D crystal that is pinned on inhomogeneities in the random potential.

5.3. Effect of the electric field

We must now consider the effect of the electric field on the properties of the S-line, observed during Wigner crystallization. It has been found that there is a threshold for the increase in the intensity of this line, which is accompanied by the appearance of additional noise due to the luminescence-signal instability near the threshold.[94] These features are explained by the disruption of the Wigner crystal pinned down by the electric field. Moreover, by varying the electric field, it is possible to isolate the S-line independently of the main luminescence signal, and thus investigate its properties. The Wigner crystal has been shown to melt in two stages that can be characterized by two critical temperatures T_{c1} and T_{c2}.

Figure 17a shows the luminescence spectra of a single heterojunction with 2D electron concentration 5.5×10^{10} cm^{-2} in a magnetic field of 16 T ($\nu=0.135$) for different potential differences, namely, $V=0$ and $V=5$ mV (electric field 0.02 V cm^{-1}). For $V=0$, the luminescence spectrum contains both the main L-line and the S-line shifted toward lower energies. In a weak electric field, the spectrum is modified: the S-line intensity is much higher whereas the L-line intensity remains unaltered. This was used to sepa-

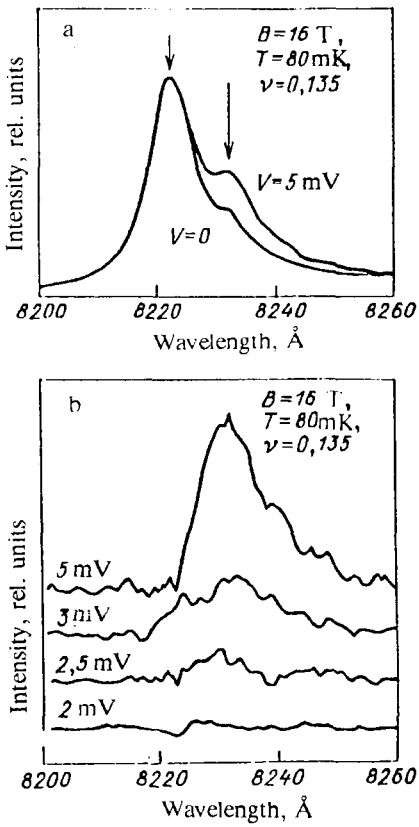

FIG. 17. (a)—Luminescence spectrum for $H=16$ T and $T=80$ mK, measured in zero and other electric fields. (b)—Differential luminescence spectra with modulated electric field.

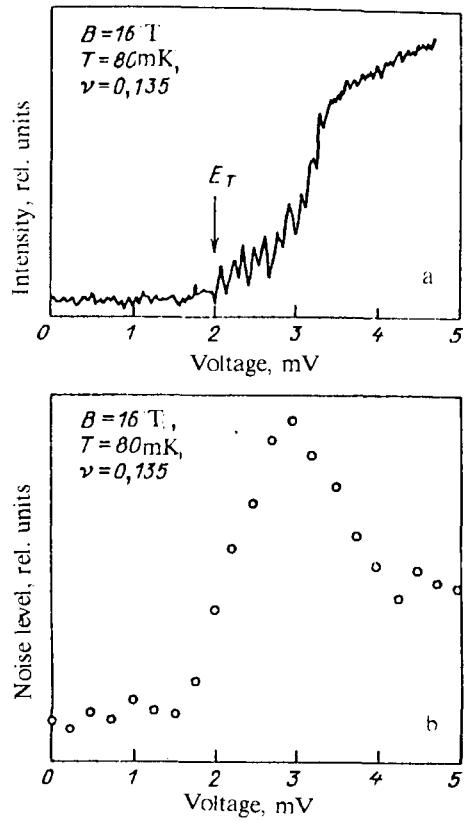

FIG. 18. S-line intensity (a) and noise level (b), recorded in differential spectra using a modulated electric field.

rate out the S-line in the differential luminescence spectra by modulating the electric field. Figure 17b shows the differential spectra obtained for different voltage modulation amplitudes. As can be seen, only the S-line is present.

Figure 18 shows the S-line intensity as a function of the voltage amplitude. The function has a threshold character: a rapid rise in the luminescence signal is observed when the voltage exceeds 2 mV. We note that the differential signal becomes very unstable near the threshold voltage. Figure 18b shows the noise level associated with the luminescence signal, measured as the root mean square deviation from the mean, as a function of the applied voltage. It is clear the noise level is much greater near the threshold. The threshold behavior of the signal and noise is correlated with the nonlinear behavior of the current-voltage characteristic,[19] and also with the generation of electric noise near the threshold. This is interpreted as the depinning of the Wigner crystal by the electric field. In this case, the depinning of the Wigner crystal produces an increase in the luminescence signal. This is said to occur because recombination of 2D electrons in the pinned Wigner crystal is less effective. In a strong magnetic field, the size of the wave function of a 2D electron is equal to the magnetic length. Holes participating in recombination are also localized (the Bohr radius of an acceptor is $a_B \sim 40$ Å). We may thus conclude that the overlap of the wave functions of an electron and a hole localized in the 2D plane decreases with increasing magnetic field, which leads to a sharp reduction in the luminescence signal. The depinning of the Wigner crystal by the electric field sets the electrons in motion, which produces an increase in the recombination probability. The luminescence-signal instability near the threshold voltage is probably due to the presence of a large number of crystal domains in the system, whose dimensions vary with time. Since the threshold voltage may depend on the domain size, the observed instabilities near the threshold voltage are not surprising. By direct analogy with the depinning of a charge-density wave by an electric field, the threshold can be used in this case to estimate the coherence length or the linear size of 2D domains. Such estimates yield $L \leqslant 1$ μm (the number of 2D electrons per domain is $\leqslant 1000$).

5.4. Critical temperature

Figure 19 shows the temperature dependence of the S-line intensity, measured for $H=16$ T ($\nu=0.135$). It is clear from this figure that, in addition to the above temperature and filling threshold, there is also a temperature threshold, namely, $T_{c1}=0.35$ K for which the luminescence intensity is found to fall abruptly. However, the S-line does not vanish altogether at $T=T_{c1}$: it persists in the spectrum up to $T_{c2}=1.2$ K. These observations show that the Wigner crystal melts in two stages. This two-stage melting was predicted theoretically in Ref. 88 where it was

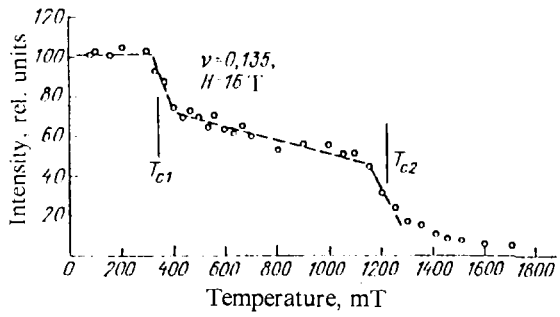

FIG. 19. S-line intensity as a function of S-line intensity, recorded using a modulated electric field. Two thresholds, T_{c1}, T_{c2} can be seen.

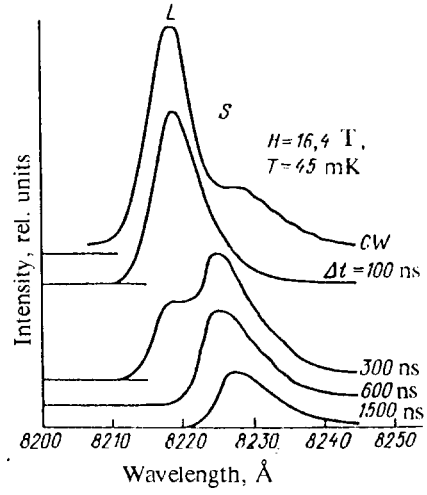

FIG. 20. Luminescence spectra of a sample with 2D electron concentration $n_s=5.3\times10^{10}$ cm^{-2}, measured using continuous-wave and pulsed excitation with different delays.

shown that the crystal to liquid crystal transition should occur at T_{c1} and the liquid crystal to liquid transition at T_{c2}. The observed depinning by the electric field for temperatures $T_{c1}<T<T_{c2}$ is in conflict with the melting model that relies on an intermediate liquid-crystal phase because the liquid crystal cannot be pinned down. Another possible explanation of the existence of two critical temperatures is provided by model numerical calculations of T_c as a function of the size of the 2D crystal.[85] According to this calculation, the critical temperature for melting of the 2D crystal decreases with increasing crystal size. It follows that T_{c2} may be the melting point of domains with a low number of electrons (of the order of 10). Magneto-optics as a local method may be sensitive to the properties of polycrystals with very small dimensions.

The two critical points T_{c1} and T_{c2} have been observed independently in magneto-optic experiments in which a study was made of the recombination of 2D electrons with free holes in a single heterojunction. These experiments revealed an analogous S-line, and its temperature properties were investigated.[75]

5.5 Kinetics of luminescence spectra and the phase diagram of the Wigner crystal

Studies of time-resolved luminescence spectra under pulsed excitation have shown that it is possible to separate in time the spectra due to liquid (L-line) and crystal (S-line) phases. This possibility relies on the fact that the radiative recombination time constants of electrons in the liquid and crystal phases are different by more than an order of magnitude.

Figure 20 shows the luminescence spectra of a sample with 2D electron concentration of 5.3×10^{10} cm^{-2} in a magnetic field of 16.4 T at $T=45$ mK. The uppermost spectrum in the figure was obtained under continuous photoexcitation and contains the two lines—L and S—that correspond to the liquid and crystal phases, respectively. The evolution of the spectra in time is shown in the lower part of the figure. For delays $\Delta t=100$ ns, the spectrum is dominated by the L line, whereas only the S line, which corresponds to the crystal phase, remains for $\Delta t=500$ ns.

The radiative time constants of the liquid and solid phases can be determined from the time dependence of the integral photoluminescence for different fields H (Fig. 21). For $H<2$ T, the intensity falls exponentially with time constant $\tau=220$ ns, which corresponds to the recombination of electrons from the liquid phase. As H increases, a long tail due to radiative damping associated with recombination from the solid phase is found to appear. The radiative time constants corresponding to this tail are shown in the insert in Fig. 21 as functions of H. From $\nu=1$ onward, τ increases monotonically, and then follows the exponential law

$$\tau=\tau_0\exp(H/H_0)=\tau_0\exp(A/\nu), \qquad (5.1)$$

where τ_0 is the recombination time constant for $H=0$ and $A\approx0.3$.

The exponential dependence of τ on H is due to the overlap of the wave functions of electrons and holes in the 2D plane. Actually, the wave function of localized electrons in the 2D layer is determined by the magnetic length: $\psi\sim\exp(-x^2/4l_0^2)$, $l_0>r_{imp}$ (acceptor radius). The largest posible electron–acceptor separation in the plane is $d=(k/n_0)^{1/2}$. Hence the probability of finding an electron and a hole at the same point in the 2D plane is given by

$$w=w_0\exp(-d^2/2l_0)=w_0\exp(-k/\nu), \qquad (5.2)$$

in agreement with the exponential behavior of $\tau(H)$.

The competition between liquid and solid phases is seen in the behavior of the luminescence intensity which reflects the relative importance of these phases. The spectrum of each of them can be investigated independently by suitably choosing the delay ($\Delta t=100$ ns and 1500 ns for the liquid and solid, respectively). This is illustrated in Fig. 22. The luminescence signal from the liquid is constant up to the critical filling factor $\nu_c=0.26$ and then falls for $\nu<\nu_c$. The peaks at $\nu=1/5$ and $1/7$ show that the quantum liquids are stable for these fractional values of ν. For the solid, the luminescence signal appears near $\nu=1$ and then rapidly increases for $\nu<\nu_c$. The intensity oscillations

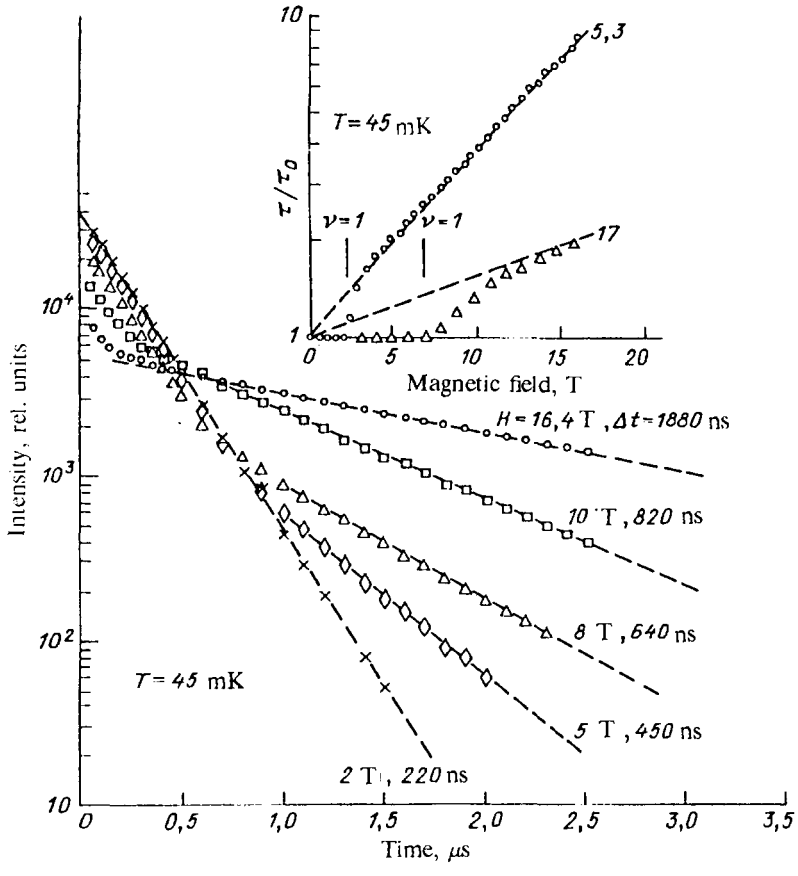

FIG. 21. Decay of luminescence intensity due to 2D electrons under pulsed excitation as a function of magnetic field. Insert shows radiative recombination time constant as a function of magnetic field H for concentrations $n_s = 5.3 \times 10^{10}$ cm^{-2} and 1.77×10^{11} cm^{-2}.

with well-defined minima at $\nu = 2/3$, 2/5, 1/3, 2/7, 2/9, 1/5, 2/11, and 1/7 are very similar to the Shubnikov magnetoresistance oscillations in FQHE.

The key to the behavior of the luminescence intensity of the solid is its temperature dependence (Fig. 23). For $T < 200$ mK, this dependence is found to exhibit a series of thresholds (indicated by the vertical bars at ν_1, ν_2, ν_3 in Fig. 23). These occur because, for $\nu \leqslant 1$, the luminescence signal corresponds to highly localized electrons due to magnetic freezeout. The electron crystal begins to emerge at $T = 200$ mK for $\nu_1 > \nu > \nu_2$ and $\nu_3 > \nu$, and the luminescence signal rises at the threshold. When $T = 40$ mK, the crystal phase occupies the wider region $\nu < \nu_c$, and the transitional behavior remains only for $\nu = 1/5$ and 1/7. In contrast to the magnetic freezing out of electrons on inhomogeneities in the random potential (extrinsic single-particle localization), the strong localization found in the case of the 2D electron crystal is intrinsic in origin.

The phase diagram of the Wigner crystal can be constructed by analysing the luminescence intensities corresponding to the liquid and solid phases. This is done by measuring the intensity as a function of temperature (insert in Fig. 23). In the neighborhood of fractional values of ν, this reveals a transitional behavior: there are sharp thresholds *near* $\nu = 1/5$ and 1/7, and no thresholds *at* these fractions.

Figure 24 shows the resulting phase diagram of the Wigner crystal. The crosses represent the critical points T_{c1} (melting) in different magnetic fields; the open circles represent the values of ν_c taken from Fig. 23. The liquid-

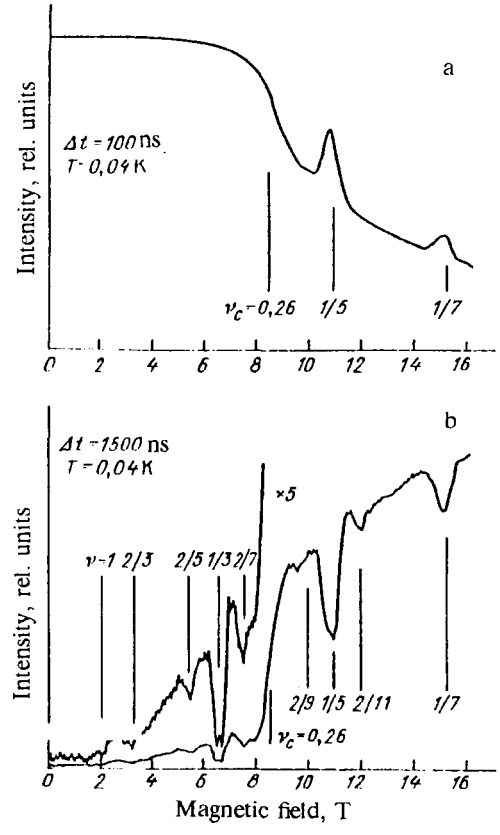

FIG. 22. Integral radiative recombination intensity as a function of magnetic field, measured for the liquid phase (a) (delay $\Delta t = 100$ ns) and solid phase (b) ($\Delta t = 1500$ ns).

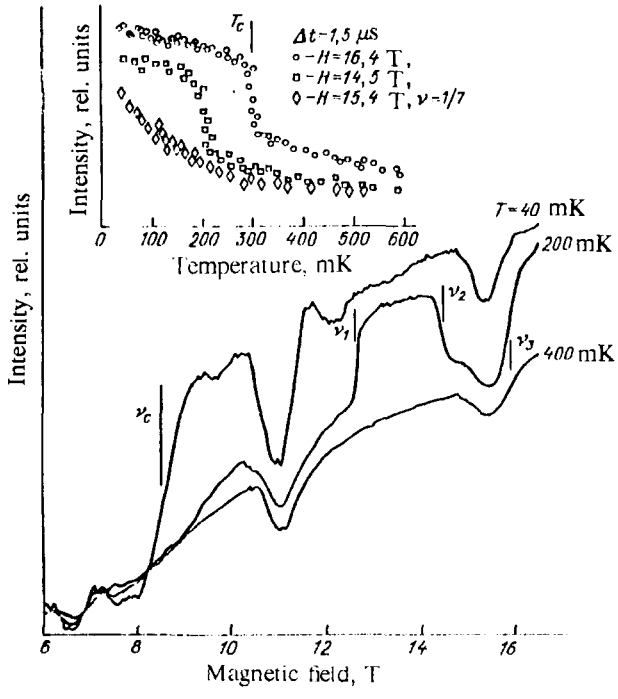

FIG. 23. Integral radiative recombination intensity due to 2D electrons in the solid (L line) as a function of magnetic field. Thresholds occur at ν_1, ν_2, and ν_3. Insert shows details of the temperature dependence of the same luminescence near $\nu=1/7$.

to-crystal transition temperature on the phase diagram is found to be lower than the classical melting point ($T=420$ mK) for the particular electron concentration. The unusual form of the phase diagram is due to the properties of the crystal/liquid-crystal/crystal transitional behavior near $\nu=1/5$ and $1/7$. For these fractional fillings, the quantum liquid is more stable than the crystal. Finally, magneto-optic measurements show that the phase boundary of the Wigner crystal begins with $\nu_c=0.26$, whereas nonlinear magneto-transport and radiofrequency absorption data suggest that $\nu_c\approx 0.22$.

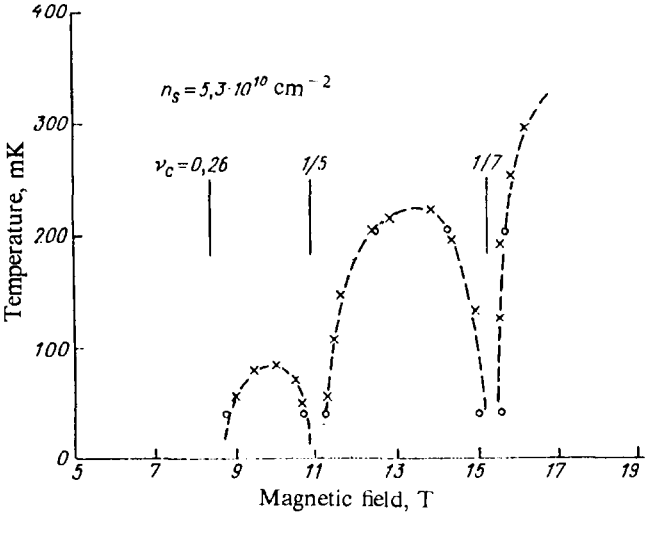

FIG. 24. Phase boundary of the Wigner crystal. Crosses and open circles represent measurements in $H=$const and $T=$const, respectively.

6. CONCLUSION

We have used the example of radiative recombination of 2D electrons with photoexcited holes to examine the possibilities of the magneto-optic approach to the experimental investigation of the ground-state energy of strongly-correlated 2D electrons in the ultra-quantum limit. The method was found to be effective in the study of Coulomb gaps and Wigner crystallization. This subject, and indeed the entire field of quantum liquids in FQHE and the crystallization of 2D electrons, is still incomplete and will continue to develop. We conclude with a resume of the most fundamental and promising avenues for future research. Magneto-optics used in conjunction with the technique of short-wave nonequilibrium acoustic phonons can be successful in direct studies of positional long-range order in systems of 2D electrons, and also in investigations of the 2D crystal to liquid phase transition itself. The techniques of correlation optics can be effective in studies of quasiparticle excitations in FQHE, and also of states such as the 'electron glass' that arise in the case of strong localization of 2D electrons on fluctuations in the random potential.

[1] K. von Klitzing, G. Dorda, and M. Pepper, Phys. Rev. Lett. **45**, 494 (1980).
[2] D. C. Tsui, H. L. Störmer, and A. C. Gossard, Phys. Rev. Lett. **48**, 1559 (1982).
[3] R. E. Prange and S. M. Girvin (editors), *The Quantum Hall Effect*, Springer-Verlag, Berlin, 1988.
[4] T. Ando, A. Fowler, and F. Stern, Rev. Mod. Phys. **54**, 437 (1982).
[5] E. I. Rashba and V. B. Timofeev, Fiz. Tekh. Poluprovodn. **20**, 977 (1986) [Sov. Phys. Semicond. **20**, 617 (1986)].
[6] E. P. Wigner, Phys. Rev. **46**, 1002 (1934).
[7] C. C. Grimes and G. Adams, Phys. Rev. Lett. **42**, 1559 (1979).
[8] R. B. Laughlin, Phys. Rev. Lett. **50**, 1395 (1983).
[9] R. B. Laughlin, Surf. Sci. **142**, 163 (1984).
[10] G. S. Boebinger, H. L. Störmer, D. C. Tsui, A. M. Chang, J. C. M. Hwang, A. Y. Cho, C. W. Tu, and W. Wiegmann, Phys. Rev. B **36**, 7919 (1987).
[11] R. L. Willett, H. L. Störmer, D. C. Tsui, A. C. Gossard, and J. H. English, Phys. Rev. B **37**, 8476 (1988).
[12] F. D. M. Haldane, Phys. Rev. Lett. **55**, 2095 (1983).
[13] G. J. Halperin, Helv. Phys. Acta **56**, 75 (1983).
[14] J. Eisenstein, H. L. Störmer, L. Pfeiffer, K. W. West, Phys. Rev. Lett. **62**, 1540 (1989); Surf. Sci. **229**, 21 (1990).
[15] T. Chakrahorty and P. Pietilainen, *Fractional Quantum Hall Effect*, Springer-Verlag, New York, 1988.
[16] P. K. Lam and S. M. Girvin, Phys. Rev. B **30**, 483 (1984).
[17] E. Y. Andrei, G. Deville, D. C. Glatti, F. I. B. Williams, E. Paris, and B. Etienne, Phys. Rev. Lett. **60**, 2765 (1988); **62**, 973 (1989).
[18] H. W. Jiang, R. Willet, H. L. Störmer, D. C. Tsui, L. N. Pfeiffer, and K. W. West, Phys. Rev. Lett. **65**, 333 (1990).
[19] V. J. Goldman, M. Santos, M. Shayegan, and J. E. Gunnimgham, Phys. Rev. Lett. **65**, 2189 (1990).
[20] R. J. Willet, M. A. Paalanen, L. N. Pfeiffer, K. W. West, R. R. Ruel, and D. J. Bishop, Proc. Internat. Conf. AHMFSF-7, Würzburg, 1990, p. 111.
[21] H. Buhmann, W. Joss, K. von Klitzing, I. V. Kukushkin, A. S. Plaut, A. S. Martines, K. Ploog, and V. B. Tomofeev, Phys. Rev. Lett. **65**, 1056 (1990); **66**, 926.
[22] I. V. Kukushkin and V. B. Timofeev, Pis'ma Zh. Eksp. Teor. Fiz. **40**, 413 (1984) [JETP Lett. **40**, 1231 (1984)].
[23] I. V. Kukushkin and V. B. Timofeev, Pis'ma Zh. Eksp. Teor. Fiz. **65**, 258 (1987) [JETP Lett. **65**, 146 (1987)].

[24] I. V. Kukushkin, V. B. Timofeev, K. von Klitzing, and K. Ploog,
[25] I. V. Kukushkin and V. B. Timofeev, Sov. Sci. Rev. A **11**, 1 (1989).
[26] I. V. Kukushkin, S. V. Meshkov, and V. B. Timofeev, Usp. Fiz. Nauk **155**, 219 (1988) [Sov. Phys. Usp. **31**, 511 (1988)].
[27] J. M. Worlock, A. C. Maciel, A. Petrou, C. H. Perry, R. L. Agarwal, M. Smith, A. C. Gossard, and W. Wiegmann, Surf. Sci. **142**, 486 (1984).
[28] A. Pinczuk, J. Shah, H. L. Störmer, R. C. Miller, A. C. Gossard, and W. Wiegmann, Surf. Sci. **142**, 492 (1984).
[29] J. C. Maan, Optical Properties of Semiconductors, edited by G. Martinez, NATO ASI Series, **228**, 181 (1993).
[30] K. Ploog and A, Fischer, Appl. Phys. Lett. **48**, 1392 (1986).
[31] I. V. Kukushkin, K. von Klitzing, and K. Ploog, Phys. Rev. B **37**, 8509 (1988).
[32] I. V. Kukushkin, K. von Klitzing, and K. Ploog, Phys. Rev. B **40**, 7788 (1989).
[33] J. C. Hensel, T. C. Phillips, and G. A. Thomas, **32**, 87 (1987).
[34] A. F. Dite, K. von Klitzing, I. V. Kukushkin, V. B. Timofeev, and A. I. Filin, Pis'ma Zh. Eksp. Teor. Fiz. **54**, 393 (1991) [JETP Lett. **54**, 389 (1991)].
[35] M. Dahl, D. Heiman, A. Pinczuk *et al.* Proc. EP2DS-9, Nara, 1991, p. 607.
[36] I. V. Kukushkin, K. von Klitzing, K. Ploog, V. Kirpichev, and B. Shepel', Phys. Rev. B **40**, 4179 (1988).
[37] V. V. Bel'kov and F. G. Pikus, Pis'ma Zh. Eksp. Teor. Fiz. **54**, 487 (1991) [JETP Lett. **54**, 457 (1991)].
[38] I. V. Kukushkin, Sol. State Commun. **65**, 1475 (1988).
[39] I. V. Kukushkin, Pis'ma Zh. Eksp. Teor. Fiz. **45**, 222 (1987) [JETP Lett. **45**, 276 (1987)].
[40] A. I. Filin, A. F. Dite, K. von Klitzing, I. V. Kukushkin, and O. V. Volkov, Pis'ma Zh. Eksp. Teor. Fiz. **56**, 160 (1992) [JETP Lett. **56**, 156 (1992)].
[41] A. F. Dite, K. von Klitzing, I. V. Kukushkin, V. B. Timofeev, and A. I. Filin, Pis'ma Zh. Eksp. Teor. Fiz. **54**, 635 (1991) [JETP Lett. **54**, 642 (1991)].
[42] I. V. Kukushkin, K. vom Klitzing, and K. Ploog, Phys. Rev. B **37**, 8509 (1988).
[43] W. Chen, M. Fritze, A. V. Nurmikko *et al.* **664**, 2434 (1990).
[44] A. J. Turberfield, S. R. Haynes, P. A. Wright *et al.*, **65**, 637 (1990).
[45] V. E. Kirpichev, K. von Klitzing, I. V. Kukushkin, K. Ploog, V. B. Timofeev, and V. I. Fal'ko, Pis'ma Zh. Eksp. Teor. Fiz. **54**, 630 (1991) [JETP Lett. **54**, 636 (1991)].
[46] V. E. Zhitomirskiĭ, I. E. Itskevich, V. E. Kirpichev, K. von Klitzing, I. V. Kukushkin, and V. B. Timofeev, Pis'ma Zh. Eksp. Teor. Fiz. **56**, 215 (1992) [JETP Lett. **56**, 213 (1992)].
[47] S. I. Gubarev, A. A. Dremin, K. von Klitzing *et al.* Pis'ma Zh. Eksp. Teor. Fiz. **54**, 361 (1991) [JETP Lett. **54**, 355 (1991)].
[48] G. L. J. A. Rikken *et al.*, Phys. Rev. B **34**, 5590 (1986).
[49] A. D. Wieck *et al.* B **38**, 10158 (1988).
[50] J. C. Maan, *Superlattice and Microstructure*, Springer-Verlag, Berlin, 1984, p. 184.
[51] R. Merlin, Solid State Commun. **64**, 99 (1987).
[52] V. E. Kurpichev, I. V. Kukushkin, V. B. Timofeev, and V. I. Fal'ko, Pis'ma Zh. Eksp. Teor. Fiz. **51**, 383 (1990) [JETP Lett. **51**, 436 (1990)].
[53] Yu. A. Bychkov, S. V. Iordanskiĭ, and Eliashberg, Poverkhnost' no. **10**, 33 (1982).
[54] L. D. Landau and E. M. Lifshitz, *Quantum Mechanics*, Pergamon Press, Oxford, 1976 [Russ. transl., Nauka, M., 1974, p. 752].
[55] T. Chakraborty, Phys. Rev. B **31**, 4026 (1985).
[56] F. D. M. Haldane and E. H. Rezayi, Phys. Rev. Lett. **54**, 237 (1985).
[57] S. M. Girvin, A. H. MacDonald, and P. M. Platzman, Phys. Rev. B **33**, 2481 (1986).
[58] R. Morf and B. I. Halperin, Phys. Rev. B **33**, 2221 (1986).
[59] A. H. Chang, M. A. Paalanen, D. C. Tsui, H. L. Störmer and J. C. H. Hwang, Phys. Rev. B **28**, 6133 (1983).
[60] G. S. Boebinger, A. M. Chang, H. L. Störmer, and D. C. Tsui, Phys. Rev. Lett. **55**, 1606 (1985).
[61] G. S. Boebinger, A. M. Chang, H. L. Störmer, D. C. Tsui, J. C. M. Hwang, A. Cho, C. Tu, and G. Weinmann, Surf. Sci. **170**, 129 (1986).
[62] R. L. Willett, H. L. Störmer, D. C. Tsui, A. C. Gossard, and J. H. English, Phys. Rev. B **37**, 8476 (1988).
[63] J. R. Mallet, R. G. Clark, R. J. Nicholas, R. Willett, J. J. Harris, and C. T. Foxon, Phys. Rev. B **38**, 2200 (1988).
[64] I. V. Kukushkin and V. B. Timofeev, Pis'ma Zh. Eksp. Teor. Fiz. **44**, 179 (1986)]. [JETP Lett. **44**, 228 (1986)].
[65] H. W. Jiang, H. L. Störmer, D. C. Tsui, L. N. Pfeiffer, and K. W. West, Phys. Rev. B **40**, 12013 (1989).
[66] H. W. Jiang, L. W. Engel, D. C. Tsui, H. L. Störmer, L. N. Pfeiffer, and K. W. West, Phys. Rev. B **46**, 10468 (1992).
[67] V. M. Apal'kov and E. I. Rashba, Pis'ma Zh. Eksp. Teor. Fiz. **53**, 420 (1991) [JETP Lett. **53**, 442 (1991)].
[68] F. D. M. Haldane, Phys. Rev. **51**, 605 (1983).
[69] V. M. Apal'kov and E. I. Rashba, Pis'ma Zh. Eksp. Teor. Fiz. **53**, 46 (1991) [JETP Lett. **53**, 49 (1991)].
[70] I. V. Kukushkin, N. J. Pulsford, K. von Klitzing, K. Ploog, R. J. Hang, S. Koch, and V. B. Timofeev, Europhys. Lett. **18**, 63 (1992); Phys. Rev. B **45**, 4532 (1992); Surf. Sci. **263**, 30 (1992).
[71] I. V. Kukushkin, N. J. Pulsford, K. von Klitzing, R. J. Hang, K. Ploog, H. Buhmann, M. Potemski, G. Martinez, and V. B. Timofeev, Europhys. Lett. 1993.
[72] G. Fano, F. Ortolani, and Colombo, Phys. Rev. B **34**, 2670 (1986).
[73] F. C. Zang and Das Sharma, Phys. Rev. B **33**, 2903 (1986).
[74] A. J. Turberfield, S. R. Haynes, P. A. Wright, R. A. Ford, R. G. Clark, J. F. Ryan, J. J. Harris, and C. T. Foxon, Phys. Rev. Lett. **65**, 637 (1990); Surf. Sci. **263**, 1 (1992).
[75] S. A. Brown, A. G. Davies, R. B. Dunford, E. M. Goldys, R. Newbury, R. G. Clark, P. E. Simmons, J. J. Harris, and C. T. Hoxon, Superlattices and Microstruct. **12**, 433 (1992).
[76] B. B. Goldberg, D. Heiman, A. Pinczuk, L. N. Pfeiffer, and K. W. West, Phys. Rev. Lett. **65**, 641 (1992); Surf. Sci. **263**, 243 (1992).
[77] A. Pinczuk, D. Heiman, S. Schmitt-Rink, S. L. Chuang, C. Kallin, J. P. Valladares, B. S. Dennis, L. N. Pfeiffer, and K. W. West, Proc. Twentieth ICPS, Thessaloniki, **2**, 1045 (1990).
[78] E. Wigner, **46**, 1002 (1934).
[79] C. C. Grimes, Phys. Rev. Lett. **42**, 795 (1979).
[80] G. J. Deville, Low Temp. Phys. **72**, 135 (1988).
[81] M. Imada and M. Takahashi, J. Phys. Soc. Jpn. **53**, 3770 (1984).
[82] K. Esfarjani and S. T. Chui, J. Phys. C **3**, 5825 (1991).
[83] Zhu Xuejun and G. Louie, Phys. Rev. Lett. **70**, 335 (1993).
[84] R. Price, P. M. Platzman, and He Sang, Phys. Rev. Lett. **70**, 339 (1993).
[85] R. W. Hockney and T. R. Brown, J. Phys. C **8**, 1813 (1975).
[86] J. M. Kosterlitz and D. J. Thouless, J. Phys. C **6**, 1181 (1973); *Progress in Low Temperature Physics*, edited D. F. Brewer, North-Holland, Amsterdam, **7**, 373 (1978).
[87] K. Strandburg, Rev. Mod. Phys. **60**, 1261 (1988).
[88] D. R. Nelson and B. I. Halperin, Phys. Rev. B **19**, 2457 (1979); B **21**, 5312.
[89] F. I. B. Williams, P. A. Wright, R. G. Clark, E. Y. Andrei, G. Deville, D. C. Glatti, O. Probst, B. Etienne, C. Dorin, C. T. Foxon, and J. J. Harris, Phys. Rev. Lett. **66**, 3285 (1991).
[90] H. W. Jiang, R. L. Willett, H. L. Störmer, D. C. Tsui, L. N. Pfeiffer, and K. W. West, Phys. Rev. Lett. **65**, 33 (1990).
[91] Y. P. Li, T. Sajoto, L. W. Engel, D. C. Tsui, and M. Shayegan, Phys. Rev. Lett. **67**, 1630 (1991).
[92] M. A. Paalanen, R. L. Willett, P. B. Littlewood, R. R. Ruel, K. W. West, L. N. Pfeiffer, and D. J. Bishop, preprint (1992).
[93] G. M. Summers, M. Watts, R. A. Lewis, R. J. Nicolas, J. J. Harris, and C. T. Foxon, preprint (1992).
[94] I. V. Kukushkin, N. J. Pulsford, K. von Klitzing, R. J. Haug, R. J. Coch, and V. B. Timofeev, Phys. Rev. B **45**, 4335 (1992).
[95] I. V. Kukushkin, N. J. Pulsford, K. von Klitzing, R. J. Haug, K. Ploog, and V. B. Timofeev, Europhys. Lett. (1993) (in press).
[96] M. B. Santos *et al.* Phys. Rev. Lett. **68**, 1188 (1992).

Translated by S. Chomet